Renmin Yuan et al.,

A new method for measuring the imaginary part of the atmospheric refractive index structure parameter in the urban surface layer

ACPD-14-21285-2014

The authors appreciate the three referees for their constructive comments and suggestions. The manuscript has been revised accordingly. Our point-by-point responses to these comments are provided below. The comments of the referees are printed in black and our responses following each comment in blue.

Answer to the first anonymous referee's comments:

The atmospheric refractive index structure parameter (ARISP) is studied from both theoretical and experimental perspectives. The real part of ARISP is closely related to the strength of atmospheric turbulence whereas its imaginary part determines the absorption for radiative transfer. Because of the importance, the findings reported in this paper should be useful contributions to atmospheric physics literature.

Overall, the manuscript can be easily understood. But the manuscript in its present form needs some mandatory major revisions before it is accepted for publications.

We thank the referee for his/her positive comments.

Major issues:

1) The use of English in the manuscript needs to be substantially improved. There are a number of grammatical errors and awkward phrases or sentences in the manuscript.

We've tried our best to improve the English writing in the revised manuscript, but also the revised version of the manuscript was reviewed by a native English speaker.

2) The originality of the theoretical development in the manuscript is ambiguous. Specifically, in Section 2 "Theory" it is not clear which part is the authors' original contribution. For example, it seems that the formulas and relevant explanations in Sections 2.1 and 2.2 are taken from the literature. If this is true, please delete these sections and cite the original papers.

We have deleted Section 2.1and 2.2, and keep two sub-sections Section 2.3 and 2.4, one is for the relationship between log-intensity variance and the imaginary part of the ARISP, and the other for the relationship between the structure function and the imaginary part of the ARISP. We deleted some existing equations. However, in order to ensure the continuity of the content and the readability of the article, we kept some existing equations with references. This paper is to illustrate the process of decomposing the signals measured by a large-aperture scintillometer (LAS) into high- and low-frequency parts, which are due to the real and imaginary parts of the ARISP respectively. The contribution of the imaginary part of ARISP to the received light intensity fluctuation is figured out. Then we obtained the expressions for the variance and structure function of log-intensity caused by the imaginary part of ARISP. Based on these relationships, a practical expression for the imaginary part of ARISP is deduced and can be applied to measurement data. Compared to the method proposed by Nieveen (Nieveen et al., 1998) for estimating the refractive index structure parameter of imaginary part, this method is more objective, and can give the estimation of the outer length scale of turbulence.

We have rewritten and rearranged Section 2. Please see Page 4-10.

3) For Sections 2.3 and 2.4, trivial technical details seem unnecessary. To enhance the clarity of the manuscript, Sections 2.3 and 2.4 should be rewritten.

We have rewritten Sections 2.3 and 2.4

Please see Pages 4-10.

4) In the conclusions, the value of the findings of this study should be clearly stated. The current statement about the value of this study is too generic. It should be more specific.

We have rewritten this part. In the revised manuscript, the significance of the imaginary part of ARISP is emphasized, and the potential applications of LAS measurement on aerosols are discussed. In the discussions, the differences between long-path absorption spectroscopy and the absorption measurement are also discussed due to their common ground in aerosol monitoring.

Please see Pages 15-17.

Answer to the second anonymous referee's comments:

Major Comments:
The most innovative parts of this paper are: 1) the derivation of a rather simpler expression of the imaginary part of the atmospheric refractive index structure parameter (ARISP) (also, the equation to calculate transverse wind velocity), based on results of some original papers; 2) the aerosol concentration, e.g. in an urban area, could be obtained accordingly with ordinary LAS (Large Aperture Scintillometer) observations. This would extend the LAS usages in some cities to environmental monitoring. Generally the manuscript was properly written, with clear theoretical derivations, as well as carefully designed/ operated experiments. The paper is appropriate to the journal Atmospheric Chemistry and Physics (ACP). However, the present manuscript still needs some revisions before it can be accepted for publication.

We thank the referee for his/her positive comments.

We've tried our best to improve the English writing in the revised manuscript, but also the revised version of the manuscript was reviewed by a native English speaker.

Comments for revision:
1) Some inconsistencies in, for instance, 'Conclusions' and 'Abstract'. While the 'Conclusions' part emphases aerosol effects on the imaginary part of the ARISP, the 'Abstract' also stress the effect of 'trace gases' (with selected wavelength of LAS). The scintillometer used by the authors (with wavelength 620 nm), as well as the most popular LAS's used in recent decades (with light wavelength about 850 nm to 880 nm), are all working in the atmospheric windows. These would be improper for the assessment of trace gases.

Indeed, there are some inconsistencies in 'Conclusions' and 'Abstract'. The study offers a theoretical framework, which is to measure the imaginary part of ARISP by a large-aperture scintillometer. We choose the wave band of atmospheric window with a wavelength of 620 nm, and then the imaginary part of ARISP reflects the characteristics of aerosols. This is the goal of our current work. So we mentioned this point in both the abstract and the conclusion. The theoretical framework of the paper can also be applied to the assessment of trace gas. If we choose a wavelength for absorbing a certain trace gas, then the measured imaginary part of ARISP would reflect the characteristics of this trace gas. For example, a wave with a wavelength of 940 nm can be used to monitor water vapor.

In the revised manuscript, we deleted the part about the assessment of trace gas in the abstract, and only talked about the application to the assessment of trace gas in the conclusions as a discussion.

Please see Lines 29-29 Page1, Lines 12-15 Page 17.

2) The theoretical derivation, particularly for section 2.3 and 2.4, is a little lengthy.

We have rewritten and rearranged Section 2. In the revised manuscript, just two sub-sections are kept; one is for the relationship between log-intensity variance and the imaginary part of the ARISP, and the other for the relationship between the structure function and the imaginary part of the ARISP.

Please see Section 2 in Pages 4-10.

Some formulas particularly unused symbols are better to be deleted (e.g. the 4F*(k,L) term in Eq. (1)). While the symbols used should be described clearly.

We revised the equations and gave clear descriptions for the symbols.

Please see Line 5 Pages 4.

3) In several places it mentioned that ‘the LAS observations are performed at the height of 24.5 m’. However, the scintillometer used is actually a slant path (one side 18.5 m, another 24.5 m). An effective path height is better to be used.

We conducted two experiments. During the experiments, the transmitting and receiving parts are nearly at the same height, namely, the light beam is almost horizontal. In the first experiment, the transmitting and receiving terminals are both at the 10th floor, which is 18.5m higher than the reference plane to validate the LAS with conventional measurements. In the second experiment, the transmitting and receiving terminals are both at the 12th floor, which is 24.5m higher than the reference plane. The purpose of the first experiments is to ensure the reliability of our instrument and compare the results with the other models. In the revised version, the results of the first experiment are deleted according to the referee’s comments.

4) The English writing in this manuscript need to be carefully revised. Following are only a few examples: Page 21286, line 22: ‘trace gas’ better to be ‘atmospheric trace gases’; Page 21289, line 14-22: The symbols used in Eq. 1 need to be described precisely, e.g., k is the wave number of the light wave used; z is the position along the propagation path; etc.

Thank you for some specific revising comments. We’ve already made revisions on the syntaxes that are confusing, such as the light wave number (as η) and turbulence wavenumber (κ). We now use x to represent the horizontal transmission position.

We’ve tried our best to improve the English writing in the revised manuscript, but also the revised version of the manuscript was reviewed by a native English speaker.

Page 21289, line 23-24: ‘temperature’ is also ‘conservative’? ‘passive scalars with their sources at the surface’?

It is often assumed that if there is not source or sink of heat, and no change of phase happens except at the surface, temperature can be considered as conservative. But also, temperature can be taken as passive.

The “passive” means that, turbulence exerts force on the aerosols (or temperature) and no force from the aerosols (or temperature) is done to the turbulence.

There is something confused with the statement ‘passive scalars with their sources at the surface’, and we modified the statement.

The wavelength we used in our experiments is at the atmospheric window region, and the absorption was caused by aerosols. We assume the source of aerosols is on the ground, and there’s no production of new aerosol particles. Aerosol observations in the urban area also show that the aerosol particles and the molecule of gas follow the same law of scalars such as temperature and water vapor density, which is that the aerosol number density fluctuation spectrum follows the “-5/3” law and the co-spectrum of aerosol number density and wind speed follow the “-4/3” law [Martensson et al., 2006; Vogt et al., 2011]. Therefore, we can regard the aerosols as a conservative and passive scalar.

Please see Lines 16-24, Page 4.

Page 21290, line 15: ‘by the real part’, of what? Page 21297, line 2: ‘data process’ should be ‘data processing’.

For the question “Page 21290, line 15: ‘by the real part’, of what?”, it is by the real part of the ARISP. We modified the text.

Please see Line 20 Page 5, Line 5 Page 10.

Page 21302, line 27-28: On the date and time, better to be‘...at09:00LT,15 Jan 2014, and at 12:00 LT the next day’.

According to the comments, we have rewritten the date and time as the format.

New references:
Martensson, E. M., E. D. Nilsson, G. Buzorius, and C. Johansson (2006), Eddy covariance measurements and parameterisation of traffic related particle emissions in an urban environment, *Atmos. Chem. Phys.*, *6*, 769-785.
Vogt, M., E. D. Nilsson, L. Ahlm, E. M. Martensson, and C. Johansson (2011), Seasonal and diurnal cycles of 0.25-2.5 mu m aerosol fluxes over urban Stockholm, Sweden, *Tellus Series B-Chemical And Physical Meteorology*, *63*(5), 935-951, doi:10.1111/j.1600-0889.2011.00551.x.

Answer to the third anonymous referee’s comments:

Overview:

This paper presents possibly useful advances in the application of large-aperture scintillometry (LAS) to determine refractive index structure parameters. The authors claim to present a new method to separate the contributions of atmospheric absorption (the imaginary part of the refractive index structure parameter) and atmospheric scintillation (the real part of the refractive index structure parameter). It appears that there is some new theoretical development, amongst a great deal of already published theory; the authors need to clearly distinguish their new derivations from earlier published work.

We thank the referee for his/her positive comments.

We made revisions on the theoretical part of the article, deleted the some existing equations. In the revised manuscript, we keep two sub-sections for theory Section 2.3 and 2.4; one is for the relationship between log-intensity variance and the imaginary part of the ARISP, and the other for the relationship between the structure function and the imaginary part of the ARISP. We deleted some existing equations.
This paper is to illustrate the process of decomposing the signals measured by a large-aperture scintillometer into high- and low- frequency parts, which are attributed to the real and imaginary parts of the ARISP respectively. The contribution of the imaginary part of ARISP to the received light intensity fluctuation is figured out. Then we obtained the expressions for the variance and structure function of log-intensity caused by the imaginary part of ARISP. Based on these relationships, a practical expression for the imaginary part of ARISP is deduced and can be applied to measurement data. Compared to the method proposed by Nieveen (Nieveen et al., 1998) for estimating the refractive index structure constant of imaginary part, this method is more objective, and can give the estimation of the outer length scale of turbulence.
We have rewritten and rearranged Section 2. Please see Page 4-10.

This is a potentially improved method to reject the unwanted influence of absorption on the scintillometer measurement, without relying on spectral separation (analyzing the spectrum of scintillation), enabling more accurate measurement of the real part of the refractive index structure parameter, and therefore better estimation of the sensible heat flux. Furthermore, this opens the new opportunity to measure the spatial variation of atmospheric absorption along the long measurement path, which may have applications in aerosol monitoring, and potentially trace gas monitoring. The paper could be improved by further discussion of these applications, and the subtle differences between long-path absorption spectroscopy and the absorption measurement presented here.

In the revised manuscript, we presented discussions on the potential applications of this method on the measurement for the flux of aerosols. The paper proposed a theoretical framework, which may have potential ability to obtain the flux by measuring the imaginary part of ARISP using a large-aperture scintillometer. If the wavelength used is not absorbed by gases, then it reflects the characteristic of aerosol. If the wavelength used is within a certain trace gas' absorption interval, then it reflects the characteristics of this trace gas.

The revised manuscript discussed the difference between the method proposed in this paper and long path absorption spectroscopy. As far as we know, the long path absorption spectroscopy can measure attenuation of narrow band and obtain gas concentration. The goal of our study is to measure the imaginary part of the ARISP using a LAS, and it is possible to obtain the aerosol flux. The LAS can be used to measure the high-frequency fluctuation of light intensity to obtain some information including atmospheric temperature, crosswind, aerosol and other turbulence characteristics. The advantage of the spectroscopy is to attain the narrow spectral information. But the aerosol exhibits strong wide band absorption in visible region, so, if the spectroscopy can sample the attenuated light at high rate at every narrow band, then more parameters (for example, size, and chemical composition) of aerosols may be retrieved using the current method.

Please see Lines 16-32 Page 16.

The presentation is reasonably clear, but the English needs to be improved in numerous places.

We've tried our best to improve the English writing in the revised manuscript, but also the revised version of the manuscript was reviewed by a native English speaker.

It is unclear from the paper, whether a fundamentally new approach has been derived, or more likely a variation on the already known method of spectral separation for the absorption and scintillation contributions to the measured spectrum. The auto-correlation analysis presented essentially fits two asymptotic lines to the time-delay auto-correlation – I challenge the authors to show how this is fundamentally different to determining the 'corner' frequencies shown in Fig.1, by fitting the dashed and solid lines shown – as described by the authors 'analyzing the spectrum of scintillation' (p.21301).

To my knowledge, there's no literature that clearly decompose the signals measured by large-aperture scintillometer into high and low frequency parts. Absorption was ever discussed on the influence to fast frequency part and it is considered as disturbance and removed (Solignac, 2012). Spectral separation and time-delay auto-correlation are two methods that can be used in separating the signals. The two methods are introduced and applied, and results by the two methods are same. In the revised manuscript, the method of time-delay auto-correlation is deleted in order to avoid repetition.

Based on the decomposition of the signal, the contribution from the imaginary part of ARISP is obtained, and then the expressions for the variance and structure function are deduced. So a new practical expression for imaginary part of ARISP is given.

The method used to determine the 'corner' frequency: linear regression is conducted to the rapid-change part. Practically, the data points from the fifth to the 15th point are fitted for the high frequency part; then the data points from the 400th (this scale is larger than the receiver diameter) to the 10000th is fitted for the low frequency part. The y-coordinate of the intersect point (shown in Fig. 4a in the original manuscript) is the energy of the low frequency part. According to practice, the results by this method are pretty stable.

Solignac, P. A., Brut, A., Selves, J. L., Beteille, J. P., and Gastellu-Etchegorry, J. P.: Attenuating the Absorption Contribution on C-n2 Estimates with a Large-Aperture Scintillometer, Bound-Lay. Meteorol., 143, 261-283, 10.1007/s10546-011-9692-3, 2012.

The authors have not demonstrated improved results over the aforementioned spectral analysis, using the time-delay auto-correlation, and only one 20 min period is analysed by the two separate methods; therefore, it has not been shown that the time-delay auto-correlation method has any advantage. It might be claimed that the measurement of the outer length scale of turbulence is a valuable benefit; however, the experimental performance of this measurement is not properly evaluated (again only one result is quoted, which may be considered to be approximately the measurement height, a 'rule of thumb' approximation of the outer length scale). The authors should estimate the uncertainty of their measurements. Overall, very few data are shown – Fig.4 uses a single 20 min data period, and Fig.6 & Fig. 7 show the same 24 hour period.

Time-delay auto-correlation decomposes the large aperture scintillating signals into high and low frequency parts. This is relatively easy and also able to get a pretty objective and stable value. Certainly, spectral separation can generate the same result. Comparing to the spectral separation, time-delay auto-correlation has no special advantage. We have removed the discussion about time-delay auto-correlation method in the revised manuscript.

As the referee pointed out, using this method can give the value of the outer scale of turbulence. Up until now, there is no study on getting the outer scale of turbulence based on scintillation. We have conducted some experiments to measure the outer scale over the urban underlying surface. The results showed that the outer length scale of turbulence depends on height, stability, etc. Because we only talk about the imaginary part of ARISP in the manuscript, the results for outer scale of turbulence will be discussed in other paper. So we did not present the uncertainty of measurements. In this paper, the outer scale of turbulence is only treated as a needed parameter for calculating the imaginary part of ARISP.

This manuscript gives only the results from one 20 min and two 24 hours' measurements. They are mainly for testing our proposed measuring method. More results will be given in other articles.

The LAS derived crosswind comparison is not really novel and comparison with a single cup anemometer over complex urban terrain, does not provide a scientific quantitative comparison. There is insufficient discussion of the Double-Point temperature fluctuation sensor – what is its response time? As the sensor separation is 0.8 m, it will not be able to measure the same inertial sub-range turbulence measured by the LAS; how is this frequency response mismatch dealt with? Why do this comparison, if only to say that agreement will be limited by the vastly different spatial sampling (was the LAS path length still 960 m?).

Indeed, using a LAS to get the crosswind velocity and the real part of ARIP is not novel. The original manuscript intends to ensure the reliability of our LAS experiments, so we make comparisons between a single cup anemometer and LAS measured wind speed, and the real part of the ARISP measured by DP and LAS. Generally the results are satisfying, and that means our instrument is reliable. In the revised manuscript, this part has been removed.

Please see Section 4 in Pages 13-14.

The Double-Point temperature fluctuation sensor is made by inserting two tungsten wires into an electric bridge to measure the temperature difference. Each of the tungsten wires has diameter of 5um, length of 0.8 cm, and response time of approximately 0.02s. The distance of the two arms is 0.8m, with the length within the inertial sub-range of the turbulence. In the additional comparison experiment, the LAS path length was still 960 m. The measurement of LAS is sensitive to the turbulent eddies with scale of transmitting and receiving aperture diameters; namely, it's sensitive to the eddy with 0.18m (The diameters of the lenses for transmitting and receiving are 0.18m). The scale is also within the inertial sub-range of the turbulence. From this perspective, the results from the two methods are comparable. Certainly, the turbulence measured by a LAS is the integral of the whole path, while that measured by DP is from a single position. If the turbulence is distributed uniformly, the two should be consistent. In fact, as the propagating path is not uniform, the results from a single position are different from the integral of the whole path.

Fig.5(a) is a log-log scale plot, and seeing the spread of data, the apparent noise-floor of the LAS and the curve of the data, I do not agree that the comparison is 'very good'.

We agree with the referee's opinion that the agreement of comparison is not 'very good'. In the revised manuscript, we removed the comparison in the revised version because the comparison is not really novel.

The authors ought to be able to measure and state the instrumental noise floor of the LAS (which appears to be rather poor compared to some commercial LAS instruments).

The variance ($\sigma_{lnI,Re}^{2}$) of the noise of LAS we currently built is around 2.0e-06, which is that $C_{lnI,Re}^{2}$ is less than 5e-17m$^{-2/3}$. This is indeed larger than the noise of LAS for commercial instrument（~1e-17m$^{-2/3}$）.

Please see Section 4 in Pages 13-14.

Technical Comments:

1. P.21288 Lines 16-17 please expand as this is important and useful, that the imaginary part of the ARISP contains information on inhomogeneities of the absorptions (contrast with long path spectroscopy).

The measurements of urban aerosol imaginary part carried on different places show that the mean value of urban aerosol imaginary part distributes inhomogeniously in a long period of time and a large space. In order to describe the inhomogeneity, we introduce the imaginary part structure constant of refractive index. The larger this value is, the more uneven the imaginary part of the refractive index distributed, and vice versa. We expanded the statement.

Please see Lines 14-20 Page 3

2. P.21289,L.23-4 These assumptions need careful and critical justification; the absorption media may not be conservative nor passive, and sources may be above the surface (e.g. chimney stacks)? It is unlikely that the absorption and temperature sources will have the same spatial distribution at the surface – how does this affect the application of the theory?

It is often assumed that if there is not source or sink of heat, and no change of phase happens except at the surface, temperature can be considered as conservative. But also, temperature can be taken as passive.

The "passive" means that, turbulence exerts force on the aerosols (or temperature) and no force from the aerosols (or temperature) is done to the turbulence.

The wavelength we used in our experiments is at the atmospheric window region, and the absorption was caused by aerosols. We assume the source of aerosols is on the ground, and there's no production of new aerosol particles. Aerosol observations in the urban area also show that the aerosol particles and the molecule of gas follow the same law of scalars such as temperature and water vapor density, which is that the aerosol number density fluctuation spectrum follows the "-5/3" law and the co-spectrum of aerosol number density and wind speed follow the "-4/3" law [Martensson et al., 2006; Vogt et al., 2011]. Therefore, we can regard the aerosols as a conservative and passive scalar.

It is not required that the absorption and temperature sources will have the same spatial distribution at the surface. As long as the absorption media is conservative and passive, the scalar turbulence rules can be applied to the absorption media.

According to the comments, it should be careful to give some assumption, and in the revised manuscript we added some references.

Please see Lines 16-24, Page 4.

New references:

Martensson, E. M., E. D. Nilsson, G. Buzorius, and C. Johansson (2006), Eddy covariance measurements and parameterisation of traffic related particle emissions in an urban environment, *Atmos. Chem. Phys.*, *6*, 769-785.

Vogt, M., E. D. Nilsson, L. Ahlm, E. M. Martensson, and C. Johansson (2011), Seasonal and diurnal cycles of 0.25-2.5 mu m aerosol fluxes over urban Stockholm, Sweden, *Tellus Series B-Chemical And Physical Meteorology*, *63*(5),

935-951, doi:10.1111/j.1600-0889.2011.00551.x.

3. Justify the assumption of isotropic turbulence in the urban environment (p.21290, L.9-10).

Usually the heights of the transmitting and receiving units are on the 12th floor. The signal measured by large-aperture scintillometer has a larger weight on the middle part of the propagating path which is at the height of about 24.5m over the reference plane, so we can think that it satisfies the isotropy assumption.

Please see Lines 22-24 Page 10.

4. P.21292, L.10, please justify this assumption – it appears that the variances caused by the real and imaginary parts of the ARISP will be highly correlated because of their dependence on atmospheric turbulence and crosswind speed, as shown by Eq.4 and Eq.6?

The real and imaginary parts depend highly on the atmospheric turbulence and crosswind speed, but their contributions on the measured light intensity fluctuation have high and low frequency parts. The fluctuations of high and low frequency are not correlated; namely, they are independent.

Please see Lines 3-8 Page 6.

Editorial Comments

1. P.21286, Line 25 change 'line-sight' to 'line-of-sight'.

   Done.

   Please see line 2 Page 2.

2. L.26 – rephrase, turbulence alone does absorb light.

   Done.

   The scattering of atmospheric turbulence, gas molecules and aerosol particles, as well as the absorption of gas molecules and aerosol particles.

   Please see lines 2-4 Page 2.

3. P.21287, L.6 change to 'intensity in the receiving plane'; change 'a distance' to 'some distance'.

   Done.

   Please see line 9 Page 2 and line 4 Page 2

4. L.11 change 'measure' to 'determine' (since this step is dependent on similarity theory, and is not a direct measurement).

   Done.

5. L.19 change to 'contribution of absorption'.

   Done.

6. P.21288, L.29 change to 'Finally, a brief conclusion is presented'.

   Done.

7. P.21290, L.9 (and elsewhere) change 'isotopic' to 'isotropic'.

   Done.

8. P.21293, L.1 change to 'commonly used'.

   Done.

9. Other numerous minor errors in the English language need to be addressed.

We’ve tried our best to improve the English writing in the revised manuscript, but also the revised version of the manuscript was reviewed by a native English speaker.

Finally, the authors thank the three referees for their constructive comments that help us to greatly improve the clarity and the quality of the manuscript. We sincerely hope our answers can relieve doubts and give a better description of our work.

A new method for measuring the imaginary part of refractive index structure parameter in the urban surface layer

R. Yuan[1], T.Luo[1], J. Sun[2], Z. Zeng[1], C. Ge[3], and Y.Fu[1]

[1]Key Laboratory of the Atmospheric Composition and Optical Radiation, CAS, School of Earth and Space Sciences, University of Science and Technology of China, Anhui, 230026, China

[2]School of Atmospheric Sciences, Nanjing University, Jiangsu, 210093, China

[3]Optoelectronic Engineering Laboratory, Army Officers Academy, PLA, Anhui, 230031, China

Correspondence to: R. Yuan (rmyuan@ustc.edu.cn) and T. Luo (luotao@ustc.edu.cn)

Abstract

The ~~Atmospheric~~ atmospheric refractive index consists of both ~~the~~ real and ~~the~~ imaginary parts. The intensity of refractive index fluctuations is generally~~usually~~ expressed as the refractive index structure parameter, ~~whose~~ with the real part reflects~~s~~ing the strength of the atmospheric turbulence ~~while~~ and the imaginary part ~~reflects~~ reflecting~~the~~ absorption in the light path. ~~The~~ A large aperture scintillometer (LAS) is often used to measure the structure parameter of the real part of the atmospheric refractive index, ~~and~~ from which the sensible and latent heat fluxes can further be obtained, whereas~~while~~ the influence of the imaginary part is ignored, or considered~~thought to be a~~ noise. In this theoretical analysis study,~~Based on~~ the relationship between~~expression for the spectrum of the~~ logarithmic light intensity ~~fluctuation~~ variance and the atmospheric refractive index structure parameter (ARISP)~~caused by the imaginary part of refractive index, new expressions for the logarithmic intensity fluctuation variance~~, as well as that between the~~ and the~~ logarithmic light intensity structure function and the ARISP, is derived. Additionally,~~related to the imaginary part of refractive index are derived. Then~~ a simple expression for the imaginary part of the ~~atmospheric refractive index structure parameter (~~ARISP~~)~~ is obtained,~~.~~ ~~It~~ which can be conveniently used to determine~~measure~~ the imaginary part of the ARISP from LAS measurements. Moreover, these relations provide a new method for estimating the outer scale of turbulence. ~~Experiments of l~~Light propagation experiments were performed in the urban surface layer, from which~~ and~~ the imaginary part of the ARISP was calculated. The experimental results showed ~~a~~ good agreement with the presented theory. The results also suggested that~~,~~ the imaginary part of ARISP exhibits~~shows~~ a different diurnal variation from that of the real part of ARISP. For the 0.62 µm ~~light with the~~ wavelength ~~of~~used~~ 0.62 µm~~, the variation of the imaginary part of ARISP is related to both the turbulent transport process and the spatial distribution characteristics of aerosols.

Formatted: No underline, Font color: Black

Formatted: No underline, Font color: Black

Formatted: No underline

Formatted: No underline, Font color: Black

Formatted: No underline

Formatted: No underline, Font color: Black

Formatted: No underline

Formatted: No underline, Font color: Black

Formatted: No underline

Formatted: No underline, Font color: Black

Formatted: No underline

Formatted: No underline, Font color: Black

Formatted: No underline

Formatted: No underline, Font color: Black

Formatted: No underline

Formatted: No underline, Font color: Black

Formatted: No underline

Formatted: No underline, Font color: Black

Formatted: No underline

Formatted: No underline, Font color: Black

Formatted: No underline

Formatted: No underline, Font color: Black

Formatted: No underline

Formatted: No underline, Font color: Black

Formatted: No underline

Formatted: No underline, Font color: Black

Formatted: No underline

Formatted: No underline, Font color: Black

Formatted: No underline

Formatted: No underline, Font color: Black

~~Based on the theoretical analysis, it can be expected that the method presented in this study can be applied to measuring the imaginary part of the ARISP caused by the trace gas, if the light wavelength is selected within the corresponding gas absorption region.~~

1 Introduction

~~In the atmosphere, the~~ A line-of-sight light wave propagating~~ light wave~~ in the atmosphere undergoes~~is affected by the~~ scattering by atmospheric ~~and absorption of the~~ turbulence, gas molecules and ~~the~~ aerosol particles, as well as absorption by gas molecules and aerosol particles.~~,~~ After the light propagates ~~a~~ some distance, ~~the~~ fluctuations~~ of~~ in the light intensity ~~is~~ are not only related to the inhomogeneous scattering ~~due to~~by~~ the~~ turbulence and particles~~,~~ but also ~~related~~ to the~~ir~~ absorption, occurring along the light path. According to optical propagating theory (Rao, 2012;Tatarskii, 1961), the scattering is associated with the real part of the atmospheric refractive index~~,~~ and the absorption is associated with the imaginary part. Based on the relationship between ~~the fluctuation of~~ the light intensity fluctuations ~~o~~in the receiving plane after ~~light~~ propagati~~ng~~on for ~~a~~ some distance and~~ the~~ the fluctuations of the real part of the atmospheric refractive index (Clifford, 1971;De Bruin and Evans, 2012;Wang et al., 1978), the real part of atmospheric refractive index structure parameter (ARISP) can be deduced. Under the free-convection condition, the real part of the ARISP is related to the turbulent transport of temperature and water ~~vapor~~vapour (Wyngaard et al., 1971), which allows ~~the~~ a large aperture scintillometer (LAS) to ~~measure~~ determine the sensible heat flux and latent heat flux by measuring light intensity fluctuation ~~-~~(Andreas, 1989). ~~When~~ Although~~electromagnetic wave propagates in the atmosphere,~~ absorption ~~will inevitably~~ inevitably ~~happen~~occurs when an electromagnetic wave propagates in the atmosphere,~~,~~ ~~and~~ ~~some~~certain mathematical methods can be used to remove the contribution of absorption to scintillation under weak atmospheric absorption conditions (Solignac et al., 2012). However, it is important to understand the role of absorption in observed scintillation under strong atmospheric absorption conditions, such as polluted atmospheric boundary layer or selected atmospheric absorption regions. This study aims to develop a theoretical framework to analys~~z~~e the contribution of absorption~~'s~~ ~~contribution~~ to scintillation, which can be used to derive the imaginary part of the ARISP in the urban atmospheric boundary layer from scintillation measurements.

As early as 1983, Filho et al. measured the scintillation spectra ~~from~~ of a microwave propagating ~~on~~ over a distance of 4.1 km in central London~~ city centre area~~ (Filho et al.,

Formatted: No underline, Font color: Black

Formatted: No underline, Font color: Black

Formatted: No underline, Font color: Black

Formatted: No underline

Formatted: No underline, Font color: Black

Formatted: No underline

Formatted: No underline, Font color: Black

Formatted: No underline

Formatted: No underline, Font color: Black

Formatted: No underline

Formatted: No underline, Font color: Black

Formatted: No underline

Formatted: No underline, Font color: Black

Formatted: No underline, Font color: Black

Formatted: No underline, Font color: Black

Formatted: No underline, Font color: Black

Formatted: No underline, Font color: Black

Formatted: No underline, Font color: Black

Formatted: No underline, Font color: Black

Formatted: No underline, Font color: Black

Formatted: No underline, Font color: Black

Formatted: No underline, Font color: Black

Formatted: No underline, Font color: Black

Formatted: No underline, Font color: Black

Formatted: No underline, Font color: Black

1983). The frequency of the microwave used ~~is~~ was ~~on~~ off resonance from~~the side of~~ the 60 GHz oxygen absorption peak, and the wavelength (5.4 mm) wa~~i~~s ~~far~~ much larger than the size of aerosol ~~size~~particles. ~~Results~~ Analysis showed that the lower corner frequency derived from the scintillation spectra using the method ~~predicted~~ proposed by Ott and Thompson Jr. (Ott and Thompson Jr., 1978) is very close to the O_2 absorption region, in which the scintillation~~a good approximation for the~~ is ~~enhancement~~ enhanced~~of the scintillations due to the O_2 absorption~~. This result suggests that the effect of absorption can be determined from scintillation measurements. Nieveen et al. (Nieveen et al., 1998) obtained a value of approximately $4.1\times10^{-24}m^{-2/3}$ for the imaginary part of the ARISP of ~~about $4.1\times10^{-24}m^{-2/3}$~~ at a pasture site based on ~~the~~ scintillation data collected over ~~248m~~ a distance of 248 m ~~at~~for a wavelength of 0.940μm, which lies inside a~~ water vapour~~n absorption band of water vapour. However, ~~T~~their experiments didn't measure ~~the aerosol information. Thus the~~ absorption by aerosol particles.~~cannot be identified.~~ In those studies, the imaginary part of the ARISP was obtained by the lower corner frequency in the spectral densities of light intensity fluctuations. However,~~But~~ it is difficult to objectively identify the lower corner frequency due to the variation~~s~~ of the spectral density in the low frequencies~~ of these spectral densities~~.

Limited research has been conducted on the contribution of aerosol absorption to the intensity fluctuations of light wave~~s by aerosol absorptions~~. ~~The~~ One possible reason is that~~, the~~ aerosol concentrations are very low in ~~lots of~~several areas, making~~ and thus~~ the contribution of aerosol absorption negligible~~ is too small~~. However, many developing countries are suffering from increasing aerosol pollution ~~with~~ containing a high fraction of soot ~~contributions~~. For example, many cities in China are ~~experience~~ experiencing ~~more and more~~increasingly serious fog and haze conditions, which strongly affect~~ the~~ visibility and radiation levels (Ding and Liu, 2014). ~~The s~~Soot aerosols have strong and broad absorption~~s~~ bands. A few studies have been performed to measure the mean imaginary part of the aerosol refractive index (Raut and Chazette, 2008;Zhang et al., 2013), the results of which indicate~~s~~ that the temporal and spatial distributions of the imaginary refractive index are highly variable. The~~ir~~ inhomogenities of ~~can be described by~~ the imaginary refractive index can be described by the imaginary part of the ARISP. That is, an increase in the imaginary part of the ARISP suggests an increase in the inhomogeneity of the ~~.~~imaginary refractive index, and vice versa. Therefore, ~~the~~ knowledge of the imaginary part of the ARISP can be used to further understand the temporal and spatial distributions of the imaginary refractive index and~~ the~~ aerosol transport~~ation~~.

Formatted: No underline, Font color: Black

Formatted: No underline, Font color: Black

Formatted: No underline, Font color: Black

Formatted: No underline, Font color: Black

Formatted: No underline, Font color: Black

Formatted: No underline, Font color: Black

Formatted: No underline, Font color: Black

Formatted: No underline, Font color: Black

Formatted: No underline, Font color: Black

Formatted: No underline, Font color: Black

Formatted: No underline, Font color: Black

Based on the proposed theoretical framework and the LAS experiments performed, which empoly~~at the~~ visible light~~band~~ in the urban surface layer, herein we outline the development of a new objective method ~~is developed to~~for obtaining the imaginary part of the ARISP by combining ~~the~~ light fluctuation variances and structure functions, which include~~ing~~ the contribution of the imaginary refractive index. The experiments were performed in Hefei, China. The results show that the imaginary part of the ARISP can be reliably derived by this method.

Section~~.~~ 2 presents the theoretical framework, and ~~. Sect. 3 describes~~ the experiment is described in Sect. 3. ~~Sect. 4 gives~~The experimental results are presented in Sect. 4, which show that the proposed approach is capable of providing the characteristics of the imaginary part of the ARISP in the urban boundary layer. ~~At the last~~Finally, a brief conclusion is presented.

2 ~~Theory~~Methodology based on theoretical analysis

2.1 Relationship between log-intensity variance and the imaginary part of the ARISP

~~2~~

~~When the light wave propagates through a distance in the atmosphere, the light intensity fluctuates on the receiving plane. A theoretical framework is presented here to connect the spatial and temporal spectra of log-intensity and the variances and the structure function of log-intensity with the real and imaginary parts of refractive index. Based on this framework, the imaginary part of the ARISP can be directly obtained from LAS measurements.~~

~~2.1 The spatial spectrum of the log-intensity and the spectrum of refractivity index fluctuation~~

For a planar or~~ a~~ spherical wave in ~~the~~ a slowly varying turbulence field, the two-dimensional log-intensity spectrum is (Filho et al., 1983),

$$F_{\ln I}(\kappa, L) = 8\pi\eta^2 \int_0^L \{\Phi_{n,\mathrm{Re}}(\kappa)\sin^2(\theta) + \Phi_{n,\mathrm{Im}}(\kappa)\cos^2(\theta) + \Phi_{n,\mathrm{IR}}(\kappa)\sin(2\theta)\}dx$$

~~$F_{\mathrm{lnI}}(\kappa, L) = 4F_{\chi}(\kappa, L) = 8\pi k^2 \int_0^L \{\Phi_{n,\mathrm{Re}}(\kappa)\sin^2(\theta) + \Phi_{n,\mathrm{Im}}\cos^2(\theta) + \Phi_{n,IR}\sin(2\theta)\}dz$~~ (1)

Formatted: No underline, Font color: Black

Formatted: No underline, Font color: Black

Formatted: No underline, Font color: Black

Formatted: No underline, Font color: Black

Formatted: No underline, Font color: Black

Formatted: No underline, Font color: Black

Formatted: No underline

Formatted: Normal

Formatted: No underline, Font color: Black

Formatted: Font: (Default) Times New Roman, No underline, Font color: Black

Formatted: No underline, Font color: Black

Field Code Changed

Formatted: No underline, Font color: Black

~~In Eq. (1)~~where, θ is $\kappa^2 x(L-x)/2\eta L$ for spherical wave~~,~~ or $\kappa^2(L-x)/2k$ for a plane wave (in this study, only the spherical wave case ~~is~~ was considered), ~~κ~~ κ is the wave number of the two-dimensional log-intensity spectrum and ~~η~~ k is the wave number of ~~a~~ the spherical wave, ~~z~~ x is the position ~~for~~ of the ~~wave~~ propagating wave, and L is the length of propagation path~~;~~ . Additionaly ~~Φ_n~~ Φ_n is the spectrum of the refractive index, where the subscript n denotes the refractive index, the subscripts Re and Im denote the real and the imaginary part of the refractive index respectively, and the subscript IR denotes the correlation between the real part and the imaginary part. In the following analysis, it ~~'~~is assumed that the fluctuations in the real and imaginary parts of the refractive index are not correlated ~~(Filho et al., 1983),~~ (Filho et al., 1983)~~,~~; therefore, the ~~and thus the~~ joint part can be neglected.

In the atmospheric window wave used for propagation, the absorption contribution is due to aerosols. Observations over the urban surface under unstable atmospheric stratification showed that aerosol concentration fluctuations exhibit a -2/3 power dependence and that the aerosol concentration-velocity co-spectra follow a -4/3 power law dependence (Martensson et al., 2006;Vogt et al., 2011).We can therefore simply assume that the absorption media and temperature in the atmosphere are conservative and passive scalars, with their sources at the surface, and ignore the force on the turbulence. Under this ~~Assuming~~ assumption,~~that the absorption media in the atmosphere and the temperature are conservative and passive scalars with their sources at the surface,~~ ~~$F_{n,\mathrm{Re}}$~~ $\Phi_{\mathrm{n,Re}}$ and ~~$F_{n,\mathrm{Im}}$~~ $\Phi_{\mathrm{n,Im}}$ have the same form. The widely used von Karman spectrum form for$\Phi_{\mathrm{n,Re}}$ and $\Phi_{\mathrm{n,Im}}$ is adopted in the study (Andrews and Phillips, 2005), which ~~gives~~ can be expressed as follows:

$$\Phi_{n,\mathrm{Re}}(\kappa) = 0.033 C_{n,\mathrm{Re}}^2 (\kappa^2 + \frac{1}{L_0{}^2})^{-\frac{11}{6}} e^{-\frac{\kappa^2 l_0^2}{5.92^2}}$$

~~(2)~~

$$\Phi_{n,\mathrm{Im}}(\kappa) = 0.033 C_{n,\mathrm{Im}}^2 (\kappa^2 + \frac{1}{L_0{}^2})^{-\frac{11}{6}} e^{-\frac{\kappa^2 l_0^2}{5.92^2}}$$

~~(3)~~

Here, $C_{n,\mathrm{Re}}^2$ and $C_{n,\mathrm{Im}}^2$ are the real and imaginary parts of the ARISP respectively. L_0 is the outer scale of turbulence, and l_0 is the inner scale of turbulence. Although some measurements have revealed that the turbulence often show anisotropic characteristics (Consortini.A et al.,

Formatted: No underline, Font color: Black
Formatted: No underline, Font color: Black
Formatted: No underline, Font color: Black
Formatted: No underline, Font color: Black
Formatted: Font: Italic, No underline, Font color: Black
Formatted: Font: Italic, No underline, Font color: Black
Formatted: No underline, Font color: Black
Formatted: Font: Italic, No underline, Font color: Black
Formatted: No underline, Font color: Black
Formatted: Font: Italic, No underline, Font color: Black
Formatted: No underline, Font color: Black
Formatted: No underline, Font color: Black, Not Raised by / Lowered by
Formatted: No underline, Font color: Black, Subscript
Formatted: No underline, Font color: Black
Formatted: No underline, Font color: Black
Formatted: No underline, Font color: Black
Formatted: No underline, Font color: Black
Formatted: No underline, Font color: Black
Formatted: No underline, Font color: Black
Formatted: No underline
Formatted: No underline
Formatted: No underline
Formatted: No underline, Font color: Black
Formatted: No underline, Font color: Black
Formatted: No underline, Font color: Black
Formatted: No underline, Font color: Black
Formatted: No underline, Font color: Black
Formatted: Centered
Formatted: No underline, Font color: Black
Formatted: No underline, Font color: Black
Formatted: No underline, Font color: Black
Formatted: No underline, Font color: Black
Formatted: No underline, Font color: Black
Formatted: No underline, Font color: Black

1970;Yuan et al., 2014), the isotopic turbulence assumption will still be used in this paper due to the rather high measurement level (this will be further discussed in Sect. 3.1).

~~2.2~~ Assuming isotopic turbulence,~~One dimensional temporal spectrum of the log-intensity fluctuation~~

~~T~~ the ~~one~~ one-dimensional spatial spectrum can be derived ~~from~~ bythe ~~integration~~ integrating ~~of~~ Eq.(1) ~~by~~. ~~assuming the isotopic turbulence, and then i~~It can then be converted to a temporal spectrum according to the Taylor frozen hypothesis. Considering ~~the~~ aperture-smoothing effects, the temporal spectrum caused by the real part of the ARISP can be expressed as (Nieveen et al., 1998;Clifford, 1971),

$$W_{\ln I,\mathrm{Re}}(f)=64\pi^2\eta^2\int_0^L dx\int_{2\pi f/v}^{\infty}\Phi_{n,\mathrm{Re}}(\kappa)\sin^2[\frac{\kappa^2 x(L-x)}{2\eta L}][(\kappa v)^2-(2\pi f)^2]^{-1/2}\cdot$$

~~$W_{\ln I,\mathrm{Re}}(f)=64\pi^2k^2\int_0^L dx\int_{2\pi f/v}^{\infty}\Phi_{n,\mathrm{Re}}(\kappa)\sin^2[\frac{\kappa^2 x(L-x)}{2kL}][(\kappa v)^2-(2\pi f)^2]^{-1/2}\cdot$~~

$$[\frac{2J_1(\frac{D_r\kappa x}{2L})}{D_r\kappa x/2L}]^2[\frac{2J_1(\frac{D_t\kappa(L-x)}{2L})}{D_t\kappa(L-x)/2L}]^2\kappa d\kappa$$ ~~$[\frac{2J_1(\frac{D_r\kappa z}{2L})}{D_r\kappa z/2L}]^2[\frac{2J_1(\frac{D_t\kappa(L-z)}{2L})}{D_t\kappa(L-z)/2L}]^2\kappa d\kappa$~~

(~~4~~2)

Here, D_t is the transmitting aperture diameter; D_r is the receiving aperture diameter (D_t and D_r are usually ~~same~~ identical for a LAS), v is the transverse wind speed. J_1 is the ~~first~~ first-order Bessel function.

Similarly, the temporal spectrum ~~caused by~~due to the imaginary part of the ARISP could be derived and expressed as (Nieveen et al., 1998;Clifford, 1971),

$$W_{\ln I,\mathrm{Im}}(f)=64\pi^2\eta^2\int_0^L dx\int_{2\pi f/v}^{\infty}\Phi_{n,\mathrm{Im}}(\kappa)\cos^2[\frac{\kappa^2 x(L-x)}{2\eta L}][(\kappa v)^2-(2\pi f)^2]^{-1/2}\cdot$$

~~$W_{\ln I,\mathrm{Im}}(f)=64\pi^2k^2\int_0^L dx\int_{2\pi f/v}^{\infty}d\kappa\kappa\Phi_{n,\mathrm{Im}}(\kappa)\cos^2[\frac{\kappa^2 x(L-x)}{2kL}][(\kappa v)^2-(2\pi f)^2]^{-1/2}\cdot$~~

$$[\frac{2J_1(\frac{D_r\kappa x}{2L})}{D_r\kappa x/2L}]^2[\frac{2J_1(\frac{D_t\kappa(L-x)}{2L})}{D_t\kappa(L-x)/2L}]^2\kappa d\kappa$$ ~~$[\frac{2J_1(\frac{D_r\kappa z}{2L})}{D_r\kappa z/2L}]^2[\frac{2J_1(\frac{D_t\kappa(L-z)}{2L})}{D_t\kappa(L-z)/2L}]^2$~~

(~~5~~3)

Formatted: No underline, Font color: Black

Formatted: No underline, Font color: Black

Formatted: Font: (Default) Times New Roman, No underline, Font color: Black

Formatted: No underline, Font color: Black

Formatted: No underline, Font color: Black

Formatted: No underline, Font color: Black

Field Code Changed

Field Code Changed

Field Code Changed

Formatted: No underline, Font color: Black

Formatted: No underline, Font color: Black

Formatted: No underline, Font color: Black

Formatted: No underline, Font color: Black

Formatted: No underline, Font color: Black

Formatted: No underline, Font color: Black

Field Code Changed

Field Code Changed

Field Code Changed

Formatted: No underline, Font color: Black

Numerical integration of Eqs. (2) and (3) yields the log-intensity spectrum for the real part and the imaginary parts of the ARISP, respectively.

Figure 1 ~~gives~~ shows an ~~case~~ example of the temporal spectrum of the log-intensity calculated ~~with~~ from Eqs. (2) and (3) with parameters of $C_{n,\mathrm{Re}}^2$=9.5×10^{-15}m$^{-2/3}$, $C_{n,\mathrm{Im}}^2$ =4.0×10^{-24}m$^{-2/3}$, L_0=27.1m, L=960m, D_t=D_r=0.18m~~,~~ and v=1.3m/s (~~how~~ the method used to obtain $C_{n,\mathrm{Re}}^2$, $C_{n,\mathrm{Im}}^2$ and L_0 will be ~~introduced~~ described in ~~the following text~~Sect. 3.3). The dashed and solid lines in Fig.1 represent ~~is~~ the temporal ~~spectrum~~ spectra of the log-intensity that are rela~~contribu~~ted ~~by~~ to the real and imaginary parts of the ~~refractive index~~ARISP, respectively. The sum of the contributions from the real and imaginary parts are plotted as circles, and these values correspond to the measured spectrum of the log-intensity obtained from LAS experiments. At low frequencies, the contribution of the imaginary part of the refractive index to the measured spectrum (i.e., the sum in Fig. 1) is dominant, whereas that of the real part is negligibly small. The frequency distributions of the spectral densities make it possible to assume that the real and imaginary parts are independent. This characteristic allows the contribution of the imaginary part of the refractive index to be determined from the density spectrum obtained from LAS measurements.

As shown in Fig. 1, the temporal spectrum of the log-intensity due to the real part of the refractive index ~~which~~ reaches a plateau at frequencies ~~lower than~~below 3 Hz. This property suggests that ~~The~~ the spectral density of the plateau ~~part~~ region ($WP_{lnI,Re}$~~$WP_{LnI,\mathrm{Re}}$~~) could be numerically calculated as

$$WP_{\ln I,\mathrm{Re}}=1.04L^3D_t^{-2/3}D_r^{-2/3}C_{n,\mathrm{Re}}^2v^{-1}$$ (~~6~~4)

The variance of the log-intensity can be derived from the spectrum. As shown in Fig. 1, the contribution of the real part of the refractive index to the spectrum primarily occurs at higher frequencies, whereas that of the imaginary part mainly occurs at lower frequencies. These characteristics imply that the log-intensity variances caused by the real and imaginary parts are independent. Thus, the log-intensity variances corresponding to the real and imaginary parts can be determined separately at high frequencies and low frequencies from the LAS measurements.

~~The solid line represents the temporal spectrum of the log-intensity related to the imaginary part of refractive index. The sum of both real and imaginary part contributions, presented as~~

~~the circles in Fig.1, corresponds to the measured spectrum of the log-intensity from LAS experiments. The contribution of the imaginary part of the refractive index is mainly at the lower frequencies according to Eq. (5). At the low frequencies, the spectral density contributed by the real part of the refractive index is small compared to the measured spectrum, which allow the contribution of the imaginary part of the refractive index to be determined from the measurements.~~

~~2.3 The log-intensity variances caused by the real and imaginary part of the refractive index~~

~~The log-intensity fluctuation can be decomposed into the ensemble average (A_0), the slow fluctuation (e.g. low frequency) caused by the imaginary part of the refractive index ($\tilde{A}$) and the quick fluctuation (e.g. high frequency) caused by real part of the refractive index (A'), as~~

~~$\ln I = A_0 + \tilde{A}(r) + A'(r)$~~ ~~(7)~~

~~Assuming that the variances caused by the real and imaginary parts are independent, the log-intensity variance can be derived as $\sigma_{\ln I}^2 = \overline{[A - \overline{A}]^2} = \overline{[\tilde{A} - \overline{\tilde{A}}]^2} + \overline{[A' - \overline{A'}]^2}$, and consequently,~~

~~$\sigma_{\ln I}^2 = \sigma_{\ln I,\mathrm{Re}}^2 + \sigma_{\ln I,\mathrm{Im}}^2$~~ ~~(8)~~

~~Based on Eq. (8), the measured log-intensity fluctuation variance is the sum of variances at low and high frequencies, which could be determined by integrating Eq. (4) and (5) respectively.~~

Integrating ~~of~~ Eq. (~~4~~2) ~~gives~~ yields an expression for the log-intensity variance caused by the real part of the ~~refractive index~~ARISP (Wang et al., 1978)~~, which is~~:

$$\sigma_{\ln I,\mathrm{Re}}^2 = 0.89 C_{n,\mathrm{Re}}^2 L^3 D_t^{-7/6} D_r^{-7/6}$$

(~~9~~5)

In Eq. (~~9~~5), ~~the variables~~ L, D_t and D_r are constants, ~~so~~thus $\sigma_{\ln I,\mathrm{Re}}^2$ depends only on the real part of the ARISP, $C_{n,\mathrm{Re}}^2$~~,~~. This equation ~~which~~ can be alternatively expressed as:

$$C_{n,\mathrm{Re}}^2 = 1.12 \sigma_{\ln I,\mathrm{Re}}^2 L^{-3} D_t^{7/6} D_r^{7/6}$$

(~~10~~6)

Equation (~~10~~6) is the expression commonly ~~-~~used to determine the real part of the ARISP ~~equation for~~from LAS measurements ~~and data analyses~~ (Wang et al., 1978).

Formatted: Font: (Default) Times New Roman, No underline, Font color: Black

Formatted: No underline, Font color: Black

Formatted: No underline, Font color: Black

Formatted: No underline, Font color: Black

Formatted: No underline, Font color: Black

Formatted: No underline, Font color: Black

Formatted: No underline, Font color: Black

Formatted: No underline, Font color: Black

Formatted: No underline, Font color: Black

Formatted: No underline, Font color: Black

Formatted: No underline, Font color: Black

Formatted: No underline, Font color: Black

Formatted: No underline, Font color: Black

Formatted: No underline, Font color: Black

Formatted: No underline, Font color: Black

Formatted: No underline, Font color: Black

Formatted: No underline, Font color: Black

Formatted: No underline, Font color: Black

Formatted: No underline, Font color: Black

Formatted: No underline, Font color: Black

Formatted: No underline, Font color: Black

Combining Eqs. (~~6~~4) and (~~9~~5), the transverse velocity ~~could~~ can be ~~obtained~~ writen as

$$v=\frac{1.16D_t^{1/2}D_r^{1/2}\sigma_{\ln I,\mathrm{Re}}^2}{WP_{\ln I,\mathrm{Re}}} \qquad (~~11~~7)$$

Similarly, integrating ~~of~~ Eq. (3~~5~~) ~~provides~~ yields the log-intensity variance ~~caused by~~due to the imaginary part of the ~~refractive index~~ARISP: ~~as~~

$$\sigma_{\ln I,\mathrm{Im}}^2=2.95C_{n,\mathrm{Im}}^2k^2L_0^{5/3}L \qquad (~~12~~8)$$

The form of Eq. (8) reveals that~~When fixing L and k,~~ $\sigma_{\ln I,\mathrm{Im}}^2$ depends not only on the imaginary part of the ARISP ($C_{n,\mathrm{Im}}^2$), but also on the outer scale of turbulence (L_0). The relation is a new one regarding the characteristics of absorption effects on light propagation, and it implies that $C_{n,\mathrm{Im}}^2$ and L_0 can be derived from LAS measurements when additional information can be obtained, as ~~Therefore, $C_{n,\mathrm{Im}}^2$ cannot be derived by Eq. (12) only. Determining $C_{n,\mathrm{Im}}^2$~~ will be ~~further~~ d~~iscuss~~emonstrated~~ed~~ in the next section.

~~2.4~~2.2 Relationship between the structure function and the imaginary part of the ARISP~~The structure function of the log-intensity fluctuations~~

The two-point log-intensity correlation moment ($B_{lnI}(\rho)$ ~~$B_{\ln I}(\rho)$~~) with a distance ρ is defined as (Ishimaru, 1997)

$$B_{\ln I}(\rho)=2\pi\int_0^\infty F_{\ln I}(\kappa,0)J_0(\kappa\rho)\kappa d\kappa \qquad (~~13~~9)$$

~~Here~~In the above expression, J_0 is the zero-order Bessel function.

~~With the Eq. (1), the correlation moment related to the real part of the refractive index can be expressed as (Ishimaru, 1997):~~

~~$$B_{\ln I,\mathrm{Re}}(\rho)=16\pi^2k^2\int_0^L dz\int_0^\infty \Phi_{n,\mathrm{Re}}\sin^2(\theta)J_0(\kappa\rho)\kappa d\kappa \qquad (14)$$~~

~~Similarly, the correlation moment contributed by the imaginary part of the refractive index can be written as:~~

Formatted: No underline, Font color: Black
Formatted: No underline, Font color: Black
Formatted: No underline, Font color: Black
Formatted: No underline, Font color: Black
Formatted: No underline, Font color: Black
Formatted: No underline
Formatted: No underline, Font color: Black
Formatted: No underline, Font color: Black
Formatted: No underline, Font color: Black
Formatted: No underline
Field Code Changed
Formatted: No underline
Formatted: No underline, Font color: Black
Formatted: No underline, Font color: Black
Formatted: No underline, Font color: Black
Formatted: German (Germany)
Formatted: No underline
Formatted: No underline, Font color: Black
Formatted: No underline, Font color: Black
Formatted: No underline
Formatted: No underline, Font color: Black
Formatted: No underline, Font color: Black
Formatted: No underline, Font color: Black
Formatted: No underline, Font color: Black
Formatted: No underline, Font color: Black
Formatted: No underline, Font color: Black
Formatted: No underline, Font color: Black
Formatted: No underline, Font color: Black
Formatted: No underline, Font color: Black

~~$B_{\ln I,\mathrm{Im}}(\rho)=16\pi^2k^2\int_0^L dz\int_0^\infty \Phi_{n,\mathrm{Im}}\cos^2(\theta)J_0(\kappa\rho)\kappa d\kappa$~~ ~~(15)~~

According to the relationship between the correlation moment and structure function, the structure function ($D_{lnI}(\rho)$ ~~$D_{\ln I}(r)$~~) can be ~~derived~~ expressed as

$$D_{\ln I}(r)=4p\grave{O}_0^{¥}F_{\ln I}(k,0)[1- J_0(kr)]k\,dk \qquad (1\cancel{6}0)$$

~~When consider~~Upon invoking the aperture smoothing effect, ~~the real part of~~ the log-intensity structure function due to the real part of the ARISP becomes,

$$D_{\ln I,\mathrm{Re}}(\rho)=32\pi^2\eta^2\int_0^L dx\int_0^\infty \Phi_{n,\mathrm{Re}}\sin^2(\theta)[1-J_0(\kappa\rho)][\frac{2J_1(\frac{D_r\kappa x}{2L})}{D_r\kappa x/2L}]^2[\frac{2J_1(\frac{D_t\kappa(L-x)}{2L})}{D_t\kappa(L-x)/2L}]^2\kappa d\kappa$$

~~$D_{\ln I,\mathrm{Re}}(\rho)=32\pi^2k^2\int_0^L dz\int_0^\infty \Phi_{n,\mathrm{Re}}\sin^2(\theta)[1-J_0(\kappa\rho)]\kappa d\kappa[\frac{2J_1(\frac{D_r\kappa z}{2L})}{D_r\kappa z/2L}]^2[\frac{2J_1(\frac{D_t\kappa(L-z)}{2L})}{D_t\kappa(L-z)/2L}]^2$~~ (~~17~~11)

With further derivation steps, the following simplified relationships are valid~~ated~~ under the various~~different~~ conditions stated:

$$D_{\ln I,\mathrm{Re}}(\rho)=14.8C_{n,\mathrm{Re}}^2L^3D_t^{-13/6}D_r^{-13/6}\rho^2 \qquad \rho<<D_t(or\quad D_r) \qquad (\cancel{18a}12a)$$

$$D_{\ln I,\mathrm{Re}}(\rho)=4.3C_{n,\mathrm{Re}}^2L^3D_t^{-11/6}D_r^{-11/6}\rho^{4/3} \qquad \rho<D_t(or\quad D_r) \qquad (\cancel{18b}12b)$$

$$D_{\ln I,\mathrm{Re}}(r)=1.78C_{n,\mathrm{Re}}^2L^3D_t^{-7/6}D_r^{-7/6} \qquad \rho\geq D_t(or\quad D_r) \qquad (\cancel{18c}12c)$$

Equation (12c) indicates that~~The $C_{n,\mathrm{Re}}^2$ relates to the diameters of transmitting and receiving aperture. The dashed line in Fig. 2 shows the log-intensity structure function related to the real part of the refractive index calculated with the same parameters as in Fig. 1. As shown in Fig. 2,~~ when ~~ρ is relatively small, $D_{\ln I,\mathrm{Re}}$ increases with increasing ρ, and it becomes saturated when ρ reaches to the size of~~the distance between the two points is larger than the aperture diameter~~of LAS aperture, which~~, the real part of the structure function becomes saturated (as shown in Fig.2).

~~equals to two times of the log-intensity variance caused by the $C_{n,\mathrm{Re}}^2$ (the right side of Eq. (18c) is two times the right side of Eq. (9)).~~

Formatted: No underline, Font color: Black

Formatted: No underline, Font color: Black

Formatted: No underline

Formatted: No underline, Font color: Black

Formatted: No underline, Font color: Black

Formatted: No underline, Font color: Black

Formatted: No underline, Font color: Black

Formatted: No underline, Font color: Black

Formatted: No underline, Font color: Black

Field Code Changed

Field Code Changed

Field Code Changed

Formatted: No underline, Font color: Black

Formatted: No underline, Font color: Black

Formatted: No underline, Font color: Black

Formatted: No underline, Font color: Black

Formatted: No underline, Font color: Black

Formatted: No underline, Font color: Black

Formatted: No underline, Font color: Black

Formatted: No underline, Font color: Black

Formatted: No underline

Formatted: No underline, Font color: Black

Formatted: No underline, Font color: Black

Formatted: Font: Not Italic, No underline, Font color: Black

Formatted: No underline, Font color: Black

Formatted: Font: Not Italic, No underline, Font color: Black

Formatted: No underline, Font color: Black

Formatted: No underline

Formatted: No underline

Formatted: No underline, Font color: Black

Formatted: No underline, Font color: Black

Similarly, the log-intensity structure function ~~caused by~~due to the imaginary part of the refractive index is

$$D_{\ln I,\mathrm{Im}}(\rho)=32\pi^2\eta^2\int_0^L dx\int_0^\infty \Phi_{n,\mathrm{Im}}(\kappa)\cos^2(\theta)[1-J_0(\kappa\rho)][\frac{2J_1(\frac{D_r\kappa x}{2L})}{D_r\kappa x/2L}]^2[\frac{2J_1(\frac{D_t\kappa(L-x)}{2L})}{D_t\kappa(L-x)/2L}]^2\kappa d\kappa$$

~~$D_{\ln I,\mathrm{Im}}(\rho)=32\pi^2k^2\int_0^L dz\int_0^\infty \Phi_{n,\mathrm{Im}}(\kappa)\cos^2(\theta)[1-J_0(\kappa\rho)]\kappa d\kappa[\frac{2J_1(\frac{D_r\kappa z}{2L})}{D_r\kappa z/2L}]^2[\frac{2J_1(\frac{D_t\kappa(L-z)}{2L})}{D_t\kappa(L-z)/2L}]^2$~~ - (~~19~~13)

As was the case with Eqs. (11) and (12), ~~The~~ the following simplified relationships ~~could~~ can be derived through further derivation steps:

$$D_{\ln I,\mathrm{Im}}(\rho)=8.5C_{n,\mathrm{Im}}^2k^2L\rho^{5/3} \quad (D_t(or \quad D_r)<\rho<<L_0) \qquad (~~20a~~14a)$$

$$D_{\ln I,\mathrm{Im}}(r)=2.95C_{n,\mathrm{Im}}^2k^2Lr^{7/6}L_0^{1/2} \quad (\rho\sim<L_0) \qquad (~~20b~~14b)$$

Here, ~~a~~ the relationship ~~is not given in terms of ρ when~~corresponding to the case in which ρ is less than D_t (or D_r) not given~~,~~ because under this condition the contribution of $C_{n,\mathrm{Im}}^2$ to the structure function ~~caused by $C_{n,\mathrm{Im}}^2$~~ is much ~~les~~lower~~s~~ than ~~the contribution~~that of ~~$C_{n,\mathrm{Re}}^2$,~~ $C_{n,\mathrm{Re}}^2$ (see ~~which is clearly illustrated in~~ Fig. 2).

The results obtained from the numerical integration of Eqs. (11) and (13) with the same parameters used in Fig. 1 are plotted in Fig. 2. The solid line is the contribution of $C_{n,\mathrm{Im}}^2$ to the structure function, the dashed line is contribution of $C_{n,\mathrm{Re}}^2$ and the line with circular markers is the sum of the contributions. ~~The solid line in Fig. 2 shows the structure function caused by $C_{n,\mathrm{Im}}^2$ and the hollow circle line is the sum of the contribution of $C_{n,\mathrm{Im}}^2$ and $C_{n,\mathrm{Re}}^2$. It is obvious that contribution to the structure function caused by $C_{n,\mathrm{Im}}^2$ is much less than by $C_{n,\mathrm{Re}}^2$ when ρ is less than D_t (or D_r). When ρ is larger than the aperture diameter and far smaller than the outer scale, Eq. (20) indicates that the $D_{\ln I,\mathrm{Im}}$ depends only on $C_{n,\mathrm{Im}}^2$. However, the uncertainty in calculating the imaginary part of the log-intensity structure function is relatively large because the contribution from $C_{n,\mathrm{Re}}^2$ dominates when ρ is smaller than the outer scale L_0. When ρ is close to the outer scale L_0, the contribution from $C_{n,\mathrm{Im}}^2$ can be easily identified, as shown in~~

Formatted: No underline, Font color: Black

Field Code Changed

Formatted: No underline, Font color: Black

Field Code Changed

Formatted: No underline

Formatted: No underline, Font color: Black

Formatted: No underline, Font color: Black

Formatted: No underline, Font color: Black

Formatted: No underline, Font color: Black

Formatted: No underline, Font color: Black

Formatted: No underline, Font color: Black

Field Code Changed

Formatted: No underline, Font color: Black

Formatted: No underline, Font color: Black

Formatted: No underline, Font color: Black

Field Code Changed

Formatted: No underline, Font color: Black

Formatted: No underline

Field Code Changed

Formatted: No underline

Field Code Changed

Formatted: No underline

Formatted: No underline, Font color: Black

Formatted: No underline, Font color: Black

Formatted: No underline, Font color: Black

Formatted: No underline, Font color: Black

Formatted: No underline, Font color: Black

Formatted: No underline, Font color: Black

Formatted: No underline, Font color: Black

Formatted: No underline, Font color: Black

Formatted: No underline, Font color: Black

Formatted: No underline, Font color: Black

~~Fig. 2. Therefore, to reduce the noise and select a proper ρ (ρ should be close to L_0 but less than L_0), the Eq. (20b) can be used to determine $C_{n,\mathrm{Im}}^2$.~~

~~Combing eq. (20b) and (12), we get~~

$$\cancel{C_{n,\mathrm{Im}}^2 = \frac{1}{2.95\,(\sigma_{\ln I,\mathrm{Im}}^2)^{3/7}k^2 L\rho^{5/3}} D_{\ln I,\mathrm{Im}}^{10/7}} \qquad \text{(21)}$$

$$\cancel{L_0 = (\sigma_{\ln I,\mathrm{Im}}^2 / D_{\ln I,\mathrm{Im}})^{6/7}\rho} \qquad \text{(22)}$$

~~Equations (21) and (22) will be used to calculate the imaginary part of the ARISP $C_{n,\mathrm{Im}}^2$ and the outer scale L_0.~~

~~Based on the previous spectrum analysis, when ρ is larger than the aperture diameter, the contribution to the structure function from $C_{n,\mathrm{Re}}^2$ becomes saturated, which equals to two times of the log-intensity variance caused by $C_{n,\mathrm{Re}}^2$. Therefore, the structure function caused by $C_{n,\mathrm{Im}}^2$ can be derived by subtracting two times of the log-intensity variance caused by $C_{n,\mathrm{Re}}^2$ from the measured one.~~

According to Eqs. (~~7~~1) and (10), ~~, the structure function could be presented as $D_{\ln I}(\rho) = [\overline{\tilde{A}(r+\rho) + A'(r+\rho) - \tilde{A}(r) - A'(r)]^2}$, and further as~~ $D_{\ln I}(\rho) = D_{\ln I,\mathrm{Im}}(\rho) + D_{\ln I,\mathrm{Re}}(\rho)$. When ρ is relatively small, $D_{lnI,Re}$ increases with increasing ρ and becomes saturated when the value of ρ reaches that of the LAS aperture diameter. The contribution of $C_{n,\mathrm{Im}}^2$ to the structure function is much smaller than that of $C_{n,\mathrm{Re}}^2$ when ρ is less than D_t (or D_r). When ρ is larger than the aperture diameter and much smaller than the outer scale, $D_{lnI,Im}$ depends only on $C_{n,\mathrm{Im}}^2$, as expressed in Eq. (14a). However, the uncertainty in calculating $D_{lnI,Im}$ is relatively large because the contribution from $C_{n,\mathrm{Re}}^2$ dominates when ρ is smaller than L_0. When ρ is close to L_0, the contribution from $C_{n,\mathrm{Im}}^2$ is relatively large and can be easily identified. Therefore, to reduce the noise, a proper range of ρ should be selected (ρ should be close to L_0 but less than L_0), and Eq. (14b) can be used to determine $C_{n,\mathrm{Im}}^2$.

Formatted: No underline, Font color: Black

Formatted: No underline, Font color: Black

Formatted: No underline, Font color: Black

Formatted: No underline, Font color: Black

Formatted: No underline, Font color: Black

Formatted: No underline, Font color: Black

Formatted: No underline, Font color: Black

Formatted: No underline, Font color: Black

Formatted: No underline, Font color: Black

Formatted: No underline, Font color: Black

Formatted: No underline, Font color: Black

Formatted: No underline, Font color: Black

Formatted: No underline, Font color: Black

Formatted: No underline, Font color: Black

Formatted: No underline

Field Code Changed

Formatted: No underline

Field Code Changed

Formatted: No underline

Field Code Changed

Formatted: No underline

Field Code Changed

Formatted: No underline

Field Code Changed

Formatted: No underline

Formatted: No underline

Field Code Changed

Formatted: No underline

The goal of this study is to calculate the log-intensity structure function due to the imaginary part of the refractive index from the LAS measurements. Based on the previous spectral analysis, when ρ is larger than the aperture diameter, the contribution of $C_{n,\mathrm{Re}}^2$ to the structure function becomes saturated and is twice as large as the log-intensity variance due to $C_{n,\mathrm{Re}}^2$ (a comparison of Eqs. (5) and (12c) gives $D_{\ln I,\mathrm{Re}}(\rho)=2\sigma_{\ln I,\mathrm{Re}}^2$). Therefore, the contribution of $C_{n,\mathrm{Im}}^2$ to the structure function can be derived by subtracting twice the log-intensity variance due to $C_{n,\mathrm{Re}}^2$ from the measured value. That is, $D_{\ln I,\mathrm{Im}}(\rho)$ = $D_{\ln I}(\rho)$-$D_{\ln I,\mathrm{Re}}(\rho)$ = $D_{\ln I,\mathrm{Im}}(\rho)$-$2\sigma_{\ln I,\mathrm{Re}}^2(\rho)$, when ρ is larger than D_t (or D_r). This relation is used to calculate the imaginary part of the structure function.

In practice, the time series of measured signals is used to calculate the structure functions. According to Taylor's hypothesis, i.e., $\rho=v\tau$, Eq. (14b) can be alternatively written as

$$D_{\ln I,\mathrm{Im}}(v\tau)=\gamma_{\ln I,\mathrm{Im}}\tau^{7/6} \qquad (\tau \sim< L_0/v) \qquad (15)$$

where

$$\gamma_{\ln I,\mathrm{Im}}=2.95C_{n,\mathrm{Im}}^2\eta^2Lv^{7/6}L_0^{1/2} \qquad (\tau \sim< L_0/v) \qquad (16)$$

Combining Eqs. (16) and (8), we obtain

$$C_{n,\mathrm{Im}}^2=\frac{1}{2.95}\frac{\gamma_{\ln I,\mathrm{Im}}{}^{10/7}}{(\sigma_{\ln I,\mathrm{Im}}^2)^{3/7}\eta^2Lv^{5/3}} \qquad (17)$$

$$L_0=(\sigma_{\ln I,\mathrm{Im}}^2/\gamma_{\ln I,\mathrm{Im}})^{6/7}v \qquad (18)$$

On the right-hand sides of Eqs. (17) and (18), all of the variables are known or can be derived from LAS measurements. Therefore, Eqs. (17) and (18) can be used to calculate the imaginary part of the ARISP and the outer scale of turbulence.

~~(23)~~

~~$D_{\ln I}(\rho)=D_{\ln I,\mathrm{Im}}(\rho)+2\sigma_{\ln I,\mathrm{Re}}^2(\rho) \quad \rho\geq D_t(or \quad D_r)$ (23’)~~

~~For measurements at one point, the transform from space to time could be performed according to the Taylor hypothesis, i.e. $\rho=v\tau$ (τ is the delay time), so we have,~~

Formatted: No underline
Formatted: No underline
Field Code Changed
Field Code Changed
Formatted: No underline
Field Code Changed
Formatted: No underline
Field Code Changed
Formatted: No underline
Field Code Changed
Formatted: No underline
Field Code Changed
Formatted: No underline
Field Code Changed
Formatted: No underline
Field Code Changed
Formatted: No underline
Formatted: No underline
Field Code Changed
Formatted: No underline
Field Code Changed
Formatted: No underline
Formatted: No underline
Field Code Changed
Formatted: No underline
Field Code Changed
Formatted: No underline
Formatted: No underline
Field Code Changed
Formatted: No underline
Formatted: No underline
Field Code Changed
Formatted: No underline
Formatted: No underline, Font color: Black
Formatted: Justified
Formatted: No underline, Font color: Black
Formatted: No underline, Font color: Black
Formatted: No underline, Font color: Black
Formatted: No underline, Font color: Black
Formatted: No underline, Font color: Black

~~$D_{\ln I,\mathrm{Im}}(v\tau)=D_{\ln \mathrm{I}}(v\tau)\text{-}2\sigma^{2}_{\ln I,\mathrm{Re}}$ $v\tau \geq D_{t}(or \quad D_{r})$ (24)~~

~~Equation (24) will be used to calculate the imaginary part of the structure function.~~

3 Experiment and data process

In this section, ~~the~~ a description of the experiments and the ~~steps of~~ data processing steps, which utilise ~~according to~~ the theory presented above, will be given.

3.1 Experimental ~~Description~~ description~~of the experiments~~

The light propagation experiments were conducted ~~in~~ on the campus of the University of Science and Technology of China (USTC). Figure 3a shows the southern area of ~~the~~ Hefei ~~city~~City, and Fig. 3b shows the experiment site o~~i~~n the USTC campus. The experimental site is representative~~s~~ of a typical urban underlying surface. The campus is surrounded by ~~heavy traffic~~ urban roads with heavy traffic. Two main roads are located at the west and north, and a viaduct run~~i~~s overhead the western road. Four-story buildings and trees occup~~ied~~y most of the campus, ~~with~~ which collectively have a mean height of 15m (a plain with a ~~this~~ height of 15 m is ~~treated~~ considered to be~~as~~ the reference plane). The experiments were carried out between ~~the~~ a 55m-high building (symbol A in Fig. 3b) and ~~the~~ a 62m-high building (symbol B in Fig. 3b), which are located at the southernmost and northernmost points of the campus~~,~~ and are seperated by ~~with~~ a distance of 960m.~~between them.~~ The transmitter was located at the southern building, and the receiver was located at the northern building, with the laser path pointing along the south-north direction. The measurements were performed ~~respectively at~~on the ~~10th and~~ 12th floor of the two buildings, ~~with~~ at a height~~s~~ of ~~18.5 m and~~ 24.5 m above the reference plane. The signal measured by a large-aperture scintillometer has a larger weight on the middle part of the propagating path (Wang et al., 1978), which is high enough to be taken as meeting the isotropy assumption (Martensson et al., 2006). For typical LAS measurements, the height is a very important physical quantity and should be carefully measured and calibrated (Evans and De Bruin, 2011). However, ~~in this study,~~ quantitatively heat flux analyses ~~are~~ were not ~~needed~~required for this study;~~,~~ therefore, the measurement heights ~~here~~ reported are simply referenc~~r~~ed to the reference plane representing the urban canopy layer.

Formatted: No underline, Font color: Black

Formatted: No underline, Font color: Black

Formatted: No underline, Font color: Black

Formatted: No underline, Font color: Black

Formatted: No underline, Font color: Black

Formatted: No underline, Font color: Black

Formatted: No underline, Font color: Black

Formatted: No underline

Formatted: No underline

Formatted: No underline

Formatted: No underline

Formatted: No underline

Formatted: No underline, Font color: Black

Formatted: No underline, Font color: Black

Formatted: No underline, Font color: Black

A meteorology high tower (symbol C in Fig. 3(b)), w~~it~~hose~~ the~~ top is 18m above the reference plane, is located near the light path. ~~The s~~Sensors for wind speed, wind direction, temperature and humidity were mounted at ~~3 ~~three levels on the tower, the uppermost level of which ~~the uppermost level ~~is at the top of the tower. The meteorological data were sampled every ~~one~~ minute, ~~and ~~averaged and saved every 20 minutes. These measurements ~~are ~~were used to derive the stability near the surface. ~~A Double-Point temperature fluctuation sensor was installed at the top of the tower. The Double-Point temperature fluctuation sensor is a widely used method to measure the temperature structure parameter (Yuan et al., 2000;Pant et al., 1999). Two thermal resistances were inserted into the two arms of an electric bridge with about 0.8m apart, and then the temperature differences were measured and processed to provide the temperature structure parameter. The temperature structure parameters measured by the Double-Point temperature fluctuation sensor were converted to the real part of ARISP to compare with the LAS measurements. The temperature differences were sampled at 100Hz, and the real part of ARISP was calculated and saved every 20 minutes.~~

The LAS is a copy of the instrument conceived by Ting-i Wang et al. (Wang et al., 1978) and was built at USTC. The transmitting and receiving aperture diameters of the LAS used ~~in ~~for the~~i~~se measurements are 0.18m. The light source is a ~~light ~~light-emitting diode (LED) modulated at 116kHz~~.~~ ~~The ~~with a wavelength ~~is at~~of 0.620 μm~~, ~~. This wavelength is only weakly absorbed ~~at which the absorption is mainly caused by aerosol comparing to the weak~~by O_3; therefore, the observed absorption is primarily due to aerosols (Brion et al., 1998;Lou et al., 2014;Nebuloni, 2005). A transmit lens converges ~~T~~the emitted light, which~~ is converged by the transmit lens and~~ propagates over 960m to the receiver.

A photo detector~~, which is~~ located at the focus of the receiving lens~~,~~ ~~converted ~~converts light intensities to electrical signals, which can be demodulated and amplified by an amplifier. The bandwidth of the amplifier is 0.002~250Hz~~.~~ and ~~The ~~the output signal is sampled at a frequency of 500Hz. The data files are saved ~~at ~~in 20-min~~ute~~ ~~blocks~~intervals.

There are seven visibility measurement sites near the experimental field, which collect~~. The~~ visibility data ~~is available ~~every 30 ~~-~~minute.s The measurements from these sites agree well with each other, which means that the visibility ~~in ~~at our experimental ~~field ~~site can be represented by data obtained at these sites.~~measurements at these sites.~~ In this study, we used ~~the~~ visibility measurements obtained at ~~6m ~~a height of 6 m acquired from the nearest site,

Formatted: No underline, Font color: Black

Formatted: No underline, Font color: Black

Formatted: No underline, Font color: Black

Formatted: No underline, Font color: Black

Formatted: No underline, Font color: Black

Formatted: No underline, Font color: Black

Formatted: No underline, Font color: Black, Not Superscript/ Subscript

Formatted: No underline, Font color: Black

Formatted: No underline, Font color: Black

Formatted: No underline, Font color: Black

Formatted: No underline, Font color: Black

Formatted: No underline, Font color: Black

which is ~~about~~ approximately 3km away from our experimental site and is marked ~~as~~ with the symbol P in Fig. 3(a).

3.2 Data analysis method and examples

According to the theory presented in ~~the~~ Sect~~.~~, 2, the real and ~~the~~ imaginary parts of the ARISP, the transverse wind speed and the turbulence outer scale can be retrieved and calculated from LAS measurements.

~~Here~~As an example, the results of the LAS observations obtained at 20-min intervals staring ~~at~~on 15 January 2014, 08:30 LT are presented. The LAS observations are collected at 24.5m above the reference plane. During the acquisition, ~~with~~ the wind speed ~~of~~ was 1.1 ms^{-1}~~ and~~, the wind direction ~~of~~ was 86° at 18m and the visibility ~~of~~ was 6.0 km. The calculated value of L_{MO}= -11m (L_{MO} is the Obukhov length) indicates that the atmosphere in the surface layer was unstably stratified.

The spectral analysis technique is used to calculate the variance at low and high frequencies. The spectrum is calculated via FFT and plotted in Fig. 4 for the 20-min series. In Fig. 4

~~Two methods are tested for calculating the energy at low and high frequencies. The first one is the time-delay autocorrelation method, and the time-delay autocorrelation function $C_{\ln I}$ with a delay time i•Δt (Δt is the sample interval, i is the data indexes) can be expressed as:~~

~~$C_{\ln I}(i\cdot\Delta t)=\frac{1}{N}\sum_{j}^{N-1}\ln I(j)\cdot\ln I(i-j)$ (25)~~

~~Here, j is also the data indexes; N is the length of the data; the delay time i•Δt is denoted as τ in Fig. 4. Figure 4a shows the results for the example case. The x-axis is the delay time τ, and the y-axis is the time-delay autocorrelation. At the upper right corner of Fig. 4a, a partial enlarged plot shows two asymptotic lines with intersection point at (0.07s, 2.59×10^{-4}). Because lnI is a non-dimensional variable, the $C_{\ln I}$ is certainly a non-dimensional variable. Figure 4a shows that the autocorrelation has the maximum of 6.68×10^{-4} when τ is close to zero. Thus the total variance of the log-intensity is 6.68×10^{-4}. When τ is smaller than 0.07s, the autocorrelation decreases rapidly with increasing τ, which is attributed to the real part of the refractive index because the real part corresponds to the high frequent fluctuation (William et al., 2007). When τ is larger than 0.07s, the autocorrelation decreases slowly with increasing τ, which is attributed to the imaginary part of the refractive index. Therefore, the~~

Formatted: No underline, Font color: Black

Formatted: No underline, Font color: Black

Formatted: No underline, Font color: Black

Formatted: No underline, Font color: Black

Formatted: No underline

Formatted: English (U.K.)

Formatted: No underline, Font color: Black

Formatted: No underline, Font color: Black

Formatted: No underline, Font color: Black

Formatted: No underline, Font color: Black

Formatted: No underline, Font color: Black

Formatted: No underline, Font color: Black

Formatted: No underline, Font color: Black

~~horizontal asymptotic line indicates that the log-intensity variance caused by the imaginary part of the refractive index is 2.59×10^{-4}. The difference of the total variances and the variance caused by the imaginary part is the variance (4.09×10^{-4}) contributed by the real part of the refractive index.~~

~~Using Eqs. (10) and (11), $C^2_{n,\mathrm{Re}}$ equals 9.5×10^{-15}m$^{-2/3}$ and the transverse wind speed is 1.3ms^{-1}. For the transverse wind speed, $WP_{lnI,Re}$ in Eq. (11) is required and will be inferred in the following part. There are many methods to retrieve the wind speed by LAS (van Dinther et al., 2013). Equation (11) is more simple and stable than the other approaches according to our results.~~

~~After calculating the energy at high frequencies, the structure function caused by the imaginary part of the refractive index can be obtained by Eq. (24) and is shown as hollow circles in Fig. 4b. It can be seen that, when the delay time is close to 1s, the calculated structure function has very large variations, because contribution caused by the imaginary part of the refractive index is almost the same order as the real part and the subtraction results in a large variation; when the delay time is larger than 10s, the structure function follows the 7/6 power law as suggested by Eq. (20b). Thus $C^2_{n,\mathrm{Im}}$=4.0×10^{-24}m$^{-2/3}$ and L_0=27.1m can be derived from Eqs. (21) and (22). With these parameters, the structure function can be calculated with Eq. (19), which is presented as the solid line in Fig. 4b. Meanwhile, the structure function calculated with Eq. (20b) is shown as the dashed line. As shown in Fig. 4b, the simplified relationship given by Eq. (20b) could predict the structure function well when τ is within 10-50s.~~

~~Figure 4c shows the comparison between the log-intensity fluctuation power spectrum and the theoretical prediction. The measurements agree well with the theoretical prediction except that measurements at high frequencies are higher than theoretical predications, which may be caused by measurement noises. With their different contributions to high and low frequency energy, the energies caused by real and imaginary part of the refractive index can be obtained by analyzing the spectrum of scintillation. As shown in Fig. 4c~~, the ~~spectrum~~ spectral density of the plateau ~~part~~ region at ~~the~~ a frequency of ~~about~~ approximately 1 Hz is $WP_{LnI,Re}$=6.3×10^{-5}. ~~The energy~~Spectral densities higher than $WP_{LnI,Re}$ ~~at the lower frequencies is~~are contributed by the imaginary part of the ~~refractive index~~ARISP and are found in the lower-frequency region, whereas those lower than $WP_{LnI,Re}$ are contributed by the real part. With the measured

Formatted: No underline, Font color: Black

Formatted: No underline, Font color: Black

Formatted: No underline, Font color: Black

Formatted: No underline, Font color: Black

Formatted: No underline, Font color: Black

Formatted: No underline, Font color: Black

Formatted: No underline, Font color: Black

Formatted: No underline, Font color: Black

Formatted: No underline, Font color: Black

Formatted: No underline

Formatted: No underline, Font color: Black

spectrum, the ~~energy~~ spectral densities at high and low frequencies can be ~~calculated~~ integrated to yield the variances of log-intensity of~~as~~ 4.07×10^{-4} and 2.49×10^{-4} respectively~~,~~ ~~which agree well with those determined by the delay autocorrelation method~~.

Using Eqs. (6) and (7), $C_{n,\mathrm{Re}}^2$ can be calculated to be $9.5\times10^{-15}\mathrm{m}^{-2/3}$, and the transverse wind speed is 1.3 ms^{-1}. Although there are several methods for retrieving the wind speed using a LAS (van Dinther et al., 2013), based on our results, Eq. (7) is simpler and more stable than the other approaches. To ensure the reliability of our LAS experiments, additional experiments were conducted to compare the results of $C_{n,\mathrm{Re}}^2$ and the transverse wind speeds obtained using other methods. Good agreement was found between the various methods employed (not shown here).

After calculating the variance at high frequencies, the structure function due to the imaginary part of the refractive index could be obtained by subtracting two times the log-intensity variance due to $C_{n,\mathrm{Re}}^2$ from the measured refractive index; this result is shown as the hollow circles in Fig. 5. It can be observed that when the delay time is close to 1 s, the calculated structure function exhibits very large variations. The subtraction results in large variations because the contribution due to the imaginary part of the refractive index is nearly of the same order as that of the real part. When the delay time is greater than 10 s, the structure function follows a 7/6 power law dependence, as suggested by Eq. (14b).Thus, the values of $C_{n,\mathrm{Im}}^2$ $=4.0\times10^{-24}\mathrm{m}^{-2/3}$ and L_0=27.1 m can be calculated from Eqs. (17) and (18). Using these parameters, the structure function can be calculated from Eq. (13) and is presented as the solid line in Fig. 5. Additionally, the structure function calculated using Eq. (14b) is shown as the dashed line. As shown in Fig. 5, the simplified relationship given by Eq. (14b) predicts the structure function well when ρ is within the range of 5.5-13.4 m (corresponding to 5-13s). The range of the ρ value based on the power range is averaged from data acquired over several days to calculate the coefficient γ in Eq. (15).

After the parameters $C_{n,\mathrm{Re}}^2$, $C_{n,\mathrm{Im}}^2$, L_0 and v are calculated, the spectral curves described by Eqs. (2) and (3) can be obtained. These curves are shown as the dashed and solid line in Fig. 4, respectively. The comparison between the log-intensity fluctuation power spectrum and the theoretical prediction shows that the measurements agree well with the prediction. However, at high frequencies, the measurements are higher than the theoretical predications, which may

Formatted: No underline
Formatted: No underline
Field Code Changed
Formatted: No underline
Formatted: No underline
Field Code Changed
Formatted: No underline
Formatted: No underline
Field Code Changed
Formatted: No underline
Field Code Changed
Formatted: No underline
Formatted: No underline
Field Code Changed
Formatted: No underline
Field Code Changed
Formatted: No underline

be due to measurement noise.~~Figure 4d shows the log intensity structure function caused by the real part of the refractive index as a function of the delay time for τ less than 0.1s. The circles represent the measurements, and the solid and dashed lines are theoretical calculations with Eqs. (17) and (18') separately. It shows clearly that the measurements are consistent with the theoretical predictions.~~

4 Results~~Results~~

~~4.1 Comparisons between LAS and meteorology tower measurements~~

~~To ensure the reliability of our LAS experiments, the real part of the ARISP and transverse wind speed from the LAS measurements are compared with independent measurements from the meteorology tower. The LAS transmitter and the receiver were installed at the height of 18.5m, which is close to the mounting height (18.0m) of cup anemometer and the Double-Point temperature fluctuation sensor. The comparison experiments were conducted during 26-29 December 2013, during which the visibility was more than 10km.~~

~~Figure 5a show the comparison of the real part of the ARISP derived from the Double-Point temperature fluctuation sensor and the LAS based on Eq. (10). The slope of the regression line is 1.09 and the correlation coefficient is 0.95. Considering the potential differences between short-range and long-path integrated measurements, this agreement is very good. However, when the turbulent intensity is weak, LAS measurements are slightly larger than those from the Double-Point temperature fluctuation sensor, which may be due to the contribution of aerosol to the real part of the ARISP during night time.~~

~~The transverse wind speed can easily be calculated from the LAS with Eq. (10) (*v* in y-axis of Fig. 5b) and compared with cup anemometer measurements ($U_{\pm}$ in x-axis of Fig. 5b) as presented in Fig. 5b. The slope of the regression line is 0.99 and the correlation coefficient is 0.96. The statistics indicate that the overall agreement is good. The transverse wind~~

Formatted: No underline, Font color: Black

Formatted: Font: Times New Roman, No underline, Font color: Black

Formatted: Font: Times New Roman, No underline, Font color: Black

Formatted: Heading 1

Formatted: No underline, Font color: Black

Formatted: Font: Times New Roman, Not Bold

Formatted: No underline, Font color: Black

Formatted: Font: Times New Roman, Not Bold

Formatted: No underline, Font color: Black

Formatted: Font: No underline, Font color: Black, (Intl) SimSun

Formatted: No underline, Font color: Black

~~speeds from LAS are slightly larger than those from the cup anemometer under low wind speed conditions.~~

~~4.2~~4~~Diurnal variations~~

As a case study, diurnal variations of the real and imaginary parts of the ARISP, as well as the visibility, wind speed and wind direction observed during 15-16 January 2014 are presented. The LAS observations are performed at the height of 24.5m. The temporal spectrum and structure function of the logarithmic light intensity acquired during these two days are shown in Figs. 6a and b, respectively. Figure 6a clearly shows that although the ~~high~~ high-frequency part of the temporal spectrum (log(f)>-2) has a pronounced diurnal cycle with a large value at noon~~. ~~, ~~But it~~this is not the case for the ~~low~~ low-frequency part. In Fig. 6b, the structure function of the logarithmic light intensity has a pronounced diurnal cycle ~~within~~ over the ~~whole~~ entire scale range, with a large value at noon and small value during the night ~~time~~hours.

Based on the theoretical framework presented in Sect.~~-~~ 2, the derived real and imaginary parts of the ARISP are shown in Figs. 7a and b. The visibilit~~y~~ies~~,~~ as well as the wind speed and wind direction are also shown in Figs. 7c and d respectively. Figure 7a shows that the real part of the ARISP exhibits~~has~~ a typical diurnal characteristic~~s~~ of the atmospheric boundary layer turbulence (Stull, 1988). The real part of the ARISP increases gradually after sunrise, then reaches the maximum at noon and approaches ~~to the~~its minimum after sunset. ~~But for~~However, the temporal evolution the imaginary part of the ARISP displays a different pattern ~~than~~ compared with the real part. The ~~maximum of the~~ imaginary part of the ARISP reached a maximum ~~occurred~~ at 09:00 LT on 15 January 2014,~~ 09:00 LT,~~ and again at 12:00 LT the ~~16 January 2014,~~next day~~ 12:00 LT~~. ~~-~~However, ~~there are also the~~ large variations of the imaginary part of the ARISP were also observed during the other periods of the day. Three ~~of~~ such large variations are labelled ~~as~~ A, B and C in Fig. 7b. Figure 7c shows that the

Formatted: Font: Times New Roman, Not Bold

Formatted: No underline, Font color: Black

Formatted: No underline, Font color: Black

Formatted: No underline, Font color: Black

Formatted: No underline, Font color: Black

Formatted: No underline, Font color: Black

Formatted: No underline, Font color: Black

Formatted: No underline, Font color: Black

Formatted: No underline, Font color: Black

Formatted: No underline, Font color: Black

Formatted: No underline, Font color: Black

Formatted: No underline, Font color: Black

Formatted: No underline, Font color: Black

Formatted: No underline, Font color: Black

Formatted: No underline, Font color: Black

Formatted: No underline, Font color: Black

Formatted: No underline, Font color: Black

Formatted: No underline, Font color: Black

Formatted: No underline, Font color: Black

Formatted: No underline, Font color: Black

Formatted: No underline, Font color: Black

Formatted: No underline, Font color: Black

Formatted: No underline, Font color: Black

Formatted: No underline, Font color: Black

Formatted: No underline, Font color: Black

Formatted: No underline, Font color: Black

Formatted: No underline, Font color: Black

Formatted: No underline, Font color: Black

Formatted: No underline, Font color: Black

Formatted: No underline, Font color: Black

Formatted: No underline, Font color: Black

Formatted: No underline, Font color: Black

Formatted: No underline, Font color: Black

Formatted: No underline, Font color: Black

Formatted: No underline, Font color: Black

Formatted: No underline, Font color: Black

Formatted: No underline, Font color: Black

Formatted: No underline, Font color: Black

visibility ~~in daytime~~ exceed~~s~~ed approximately~~about~~ 8km during the day hours and ~~is~~ was less than 8km during the night ~~time~~hours. The relative humidity during the two days was less than 60~~%,~~ %; ~~so~~ thus, the variation ~~of~~ in visibility is mainly caused by ~~near~~ near-surface aerosol variations associated with aerosol sources and vertical transport~~ation~~. During the two days, minimal near~~-~~-surface visibility typically occur at approximately~~around~~ 6:00 LT.

Figure 7d shows weak diurnal variations in both wind speed and wind direction. The prevailing direction of the wind throughout the two days ~~is~~ was between east and southeast, with the exception of a large variation ~~of~~ in the wind direction after 12:00 LT on 16 January 2014~~, 12:00 LT~~. $C_{n,\mathrm{Im}}^2$ ~~started~~ began to increase gradually at 06:00 LT on 15 January 2014~~, 06:00 LT,~~ and reached a maximum at 9:00 LT. Figures 7a and b show that the increases ~~of~~ in $C_{n,\mathrm{Im}}^2$ ~~was earlier than~~and $C_{n,\mathrm{Re}}^2$ ~~.~~began at nearly the same time (this onset time is earlier than sunrise, which occurs at 7:00 LT in winter). Figure 7d shows that the wind speed~~s~~ increased from ~~about 0.5ms^{-1} at~~ 6:00 LT to ~~about 2.5ms^{-1} at 10~~9:00 LT on 15 January 2014. It is known that turbulence is associated with not only convective turbulence but also wind shear. The early stage of increase observed for $C_{n,\mathrm{Im}}^2$ and $C_{n,\mathrm{Re}}^2$ appears to be caused by shear-induced turbulence in the urban surface layer. Naturally, the convective turbulence was enhanced after sunrise, which led to a quick increase in $C_{n,\mathrm{Im}}^2$ and $C_{n,\mathrm{Re}}^2$ in the early morning. A similar pattern was also observed on the following morning, which indicates that, as expected, turbulence controls $C_{n,\mathrm{Im}}^2$. However, after reaching a maximum at 09:00 LT on 15 January 2014, $C_{n,\mathrm{Im}}^2$ decreased gradually while $C_{n,\mathrm{Re}}^2$ continued to increase. This situation can perhaps be explained by the variation in the visibility, which also continued to increase after 9:00 LT, implying a decreasing aerosol concentration. However, the case for the late morning of the next day is different, during which both $C_{n,\mathrm{Im}}^2$ and the visibility continued to increase from 9:00 LT to 12:00 LT. There are two possible reasons for this behaviour, one of which is that $C_{n,\mathrm{Im}}^2$ was dominantly controlled by turbulence during that period.~~The increase of $C_{n,\mathrm{Im}}^2$ was almost simultaneous with wind speed increase on 16 January 2014. The variations of $C_{n,\mathrm{Im}}^2$ was~~

Formatted ...

Formatted ...

Formatted ...

Field Code Changed

Formatted ...

Field Code Changed

Formatted ...

Field Code Changed

Field Code Changed ...

Formatted: No underline, Font color: Black

Field Code Changed

Formatted: No underline, Font color: Black

Field Code Changed

Formatted: No underline, Font color: Black

~~almost following the variations of $C^2_{n,\mathrm{Re}}$ in the morning. These correlations suggest that $C^2_{n,\mathrm{Im}}$ are affected by both $C^2_{n,\mathrm{Re}}$ and wind speed. It is known that $C^2_{n,\mathrm{Re}}$ and wind associate with convective and shear turbulence respectively. This indicates that turbulence controls $C^2_{n,\mathrm{Im}}$ as expected. However, after $C^2_{n,\mathrm{Im}}$ reached maximum at 15 January 2014, 09:00 LT, $C^2_{n,\mathrm{Im}}$ decreased gradually while $C^2_{n,\mathrm{Re}}$ still increased. This situation can be explained by the variation of visibility, which still increased after 9:00, implying lower aerosol concentration. This suggests that the variation of $C^2_{n,\mathrm{Im}}$ is also linked with aerosol variations. The moments A and C correspond with sudden wind direction changes and local rush hours with traffic jam (a strong source of local aerosol production).~~ For example, ~~At~~ at point B, $C^2_{n,\mathrm{Im}}$ increased simultaneously with $C^2_{n,\mathrm{Re}}$. Another possible explanation is that $C^2_{n,\mathrm{Im}}$ was influenced by a local emission of aerosols whose variation could not be detected by the visibility measurement (because the LAS measurement site is 3 km away from the visibility measurement site). The times A and C both fall within the local traffic rush hour, which is a strong source of local aerosol production. The peak values at A, B and C suggest that $C^2_{n,\mathrm{Im}}$ are also dependent ~~controlled by both turbulence and~~on aerosol distribution~~s~~.

5 Conclusions and discussion

~~Based on~~According to the theory of light propagation, ~~the~~ fluctuations of logarithmic light intensity depend~~s~~ on both the real and the imaginary parts of the ARISP. This study focused on how to obtain the imaginary parts of the ARISP from scintillation measurements. Based on the assumption that the von Karman spectrum can be used to describe the spectrum of the imaginary part of the refractive index, ~~Then~~ the expressions of the log-intensity variance and structure function were derived, and both of them include~~the relationships among~~ the imaginary part of the ARISP.~~,~~ As expressed by Eqs. (8) and (14b), these two relations provide a method for obtaining~~variance of scintillation and structure function of logarithmic light intensity are deduced, and the expression of~~ the imaginary part of the ARISP as well as the outer scale of turbulence from LAS measurements~~is obtained~~. The good agreement observed in this study between the measured and calculated spectra of the logarithmic light intensity and the imaginary part of structure function suggests that this method is reasonable and

Formatted: No underline, Font color: Black
Field Code Changed
Formatted: No underline, Font color: Black
Field Code Changed
Formatted: No underline, Font color: Black
Field Code Changed
Formatted: No underline, Font color: Black
Field Code Changed
Field Code Changed
Formatted: No underline, Font color: Black
Field Code Changed
Formatted: No underline, Font color: Black
Field Code Changed
Formatted: No underline, Font color: Black
Formatted: No underline, Font color: Black
Field Code Changed
Field Code Changed
Formatted: No underline, Font color: Black
Formatted: No underline, Font color: Black
Formatted: No underline, Font color: Black
Field Code Changed
Formatted: No underline, Font color: Black
Field Code Changed
Formatted: No underline, Font color: Black
Field Code Changed
Formatted: No underline, Font color: Black
Field Code Changed
Formatted: No underline, Font color: Black
Formatted: No underline, Font color: Black
Formatted: No underline, Font color: Black
Formatted: No underline, Font color: Black
Formatted: No underline, Font color: Black
Formatted: No underline, Font color: Black
Formatted: No underline, Font color: Black
Formatted: No underline, Font color: Black
Formatted: No underline, Font color: Black
Formatted: No underline, Font color: Black
Formatted: No underline, Font color: Black

Formatted: No underline, Font color: Black

applicable. Although the real part of the ARISP has been previously used to measure the sensitive and the latent heat fluxes by LAS, deriving the imaginary part from LAS has not been sufficiently investigated before. Therefore, the method proposed in this study can extend the application of LAS to urban environmental monitoring because the derived imaginary parts of the ARISP include information pertaining to aerosols whose concentration is much higher in many cities than in rural areas.

~~Experiments of light propagation through urban surface layer were conducted. The real part of the ARISP and transverse wind speed were obtained using the scintillation data. In the meantime, the real part of the ARISP was measured by the Double-Point temperature fluctuation sensor, and the wind speed and direction were also measured using the cup anemometer. The results show good agreement between the LAS and other methods. The calculated real part of the ARISP displays normal diurnal variation characteristics over urban overlying surface, which coincides the diurnal variation of turbulence strength.~~

Formatted: No underline, Font color: Black

Experiments of light propagation in the urban surface layer were conducted. Because~~Based on the deduced expressions, the imaginary part of the ARISP was calculated. Results showed good agreement with the theory. The diurnal variation of imaginary part of the ARISP does not show same trend as that of the real part. By analyzing the two-day variation of the imaginary part of the ARISP together with variations of the real part of the ARISP, visibility, wind speed and direction, we can find that the imaginary part of the ARISP may be influenced by both turbulence and aerosol concentration.~~

Formatted: No underline, Font color: Black

~~In this study,~~ the wavelength of the ~~used~~ light source ~~is~~ was 0.62μm,~~ and~~ the light attenuation is ~~mainly~~ primarily ~~made~~ caused by aerosols.~~,~~ ~~so t~~The imaginary part of the ARISP ~~is~~ was calculated according to our new method. The diurnal variation of the imaginary part of the ARISP is different from that of the real part. There is evidence that the imaginary part of the ARISP is associated with both the turbulence intensity and the aerosol concentration. Furthermore, the scintillation corresponding to the real part of the ARISP includes two contributions: the fluctuation of the refractive index caused by turbulence and the forward scatter caused by the aerosol particles. The scintillation corresponding to the imaginary part of the ARISP also includes two contributions: the absorption of aerosols and the scattering caused by the aerosol particles. The experimental results show that the diurnal variation of the real part of the ARISP exhibits the typical pattern of the diurnal variation of turbulence intensity, suggesting that the real part of the ARISP is dominantly controlled by turbulence,

Formatted: No underline, Font color: Black

Formatted: No underline, Font color: Black

Formatted: No underline, Font color: Black

Formatted: No underline, Font color: Black

Formatted: No underline, Font color: Black

Formatted: No underline, Font color: Black

whereas the scattering effect of aerosol particles is negligibly small. However, the information included in the imaginary part of the ARISP appears to be more complex. The absorption is dependent not only on the aerosol concentration but also on chemical composition. Additionally, the scattering effect is influenced not only by the aerosol concentration but also by the aerosol particle size distribution and the shape of the aerosol particles. Presently, it is not clear to what extent chemical composition, size distribution and particle shape can affect the imaginary part of the ARISP compared with the aerosol concentration. If the contribution of these variables is very small, the imaginary part of the ARISP is simply dependent on the aerosol concentration. However, if the contribution of these variables is relatively large, and their contributions are distinguishable, more information regarding the aerosols can be obtained. Although these problems need to be investigated further, the method proposed in this study provides a starting point.

The extinction in the transport path is caused by absorption and scattering by aerosols. The imaginary part of the ARISP represents the logarithmic light intensity fluctuations caused by the fluctuations of the extinction, which in turn should be mainly induced by fluctuations in the aerosol concentration, assuming that other conditions such as chemical composition, size distribution and shape are unchanged. It is clear that fluctuations in the aerosol concentration are associated with the aerosol concentration itself and the intensity of turbulent motion. Consequently, our experiments showed that the imaginary part of the ARISP is influenced by turbulence and changes in the aerosol concentration. With respect to measuring the extinction of the atmosphere, long path absorption spectroscopy can be used to obtain the attenuation in a narrow band and to derive the gas concentration (Fiddler et al., 2009). The advantage of the spectroscopy is to attain the narrow spectral information. The LAS method can be used to measure the high- and low-frequency fluctuations of light intensity, and more information—including atmospheric temperature, crosswind, aerosol absorption and other turbulence characteristics—can be obtained. If the employed spectroscopy can sample the attenuated light at a high rate at every narrow band, then additional aerosol parameters may be retrieved using the current method. The method developed in this study has the potential to allow for the retrieval of more information from aerosols.

Previous observations have shown that aerosol concentration fluctuations follow the characteristics of scalars (Martensson et al., 2006;Vogt et al., 2011), implying that the imaginary part of the ARISP might contain aerosol transport information similar to the relationship between the temperature structure parameter and the sensible heat flux. ~~influenced by turbulence and aerosol distribution. However, the presented method for the imaginary part of the ARISP should be valid for any other wavelength for measurements of gas absorption.~~ Our

~~Because the~~ measurement site is in Hefei ~~city~~ City, which has ~~with~~ a population of ~~about~~ approximately 3,500,000 and hosts~~, vehicles of~~ more than 500,000 vehicles. For~~ the~~ cities similar to Hefei, ~~for example~~e.g., Helsinki, Finland, vehicles are a ~~important~~ primary pollution source (Jarvi et al., 2009). The temporal variation of the imaginary part of the ARISP is well correlated with ~~time has similar trend to~~ the variation of the aerosol flux (Ripamonti et al., 2013). These pieces of evidence suggest~~Their large value happens at rush hours of 9:00 and 18:00, and the two variables vary significantly with wind direction. Evidence shows~~ that the imaginary part of the ARISP ~~is~~ can be used to measure the aerosol flux via LAS.~~an important variable which can provide information about aerosol. The results in this study indicate that the imaginary part of the ARISP can be easily derived from the LAS measurements.~~ Determining whether~~What information of aerosol does~~ the imaginary part of the ARISP represents ~~,~~ aerosol flux or concentration is an issue that~~,~~ should be investigated further.

Based on the theoretical analysis discussed herein, it can be expected that the method presented in this study can also be applied to measure the imaginary part of the ARISP caused by atmospheric trace gases, if the wavelength of light used is selected to be within the corresponding gas absorption region.

Acknowledgements

This study was supported by the National Natural Science Foundation of China (41475012~~40975006~~, 41230419, 91337213 and 41075041), Anhui National Natural Science Foundation of China (1208085MF100) and the Jiangsu Provincial Collaborative Innovation Center of Climate Change. Thanks will also be given to Dr. Guijian Liu, Yefei Yuan, Yu Wang, Guoshen Liu, Chune Shi and Renjun Zhou for their help in collecting data and preparing experiments.

Formatted: No underline, Font color: Black

Formatted: No underline, Font color: Black

Formatted: No underline, Font color: Black

Formatted: No underline, Font color: Black

Formatted: No underline, Font color: Black

Formatted: No underline, Font color: Black

Formatted: No underline, Font color: Black

Formatted: No underline, Font color: Black

Formatted: No underline, Font color: Black

Formatted: No underline, Font color: Black

Formatted: No underline, Font color: Black

Formatted: No underline, Font color: Black

Formatted: No underline, Font color: Black

Formatted: No underline, Font color: Black

Formatted: No underline, Font color: Black

Formatted: No underline, Font color: Black

Formatted: No underline, Font color: Black

Formatted: No underline, Font color: Black

Formatted: No underline, Font color: Black

Formatted: No underline, Font color: Black

Formatted: Normal

Formatted: No underline, Font color: Black

Formatted: No underline, Font color: Black

Formatted: No underline, Font color: Black

Formatted: Normal

References

Andreas, E. L.: Two-wavelength method of measuring path-averaged turbulent surface heat fluxes, J. Atmos. Ocean Tech., 6, 280-292, 1989.

Andrews, L. C., and Phillips, R. L.: Laser beam propagation through random media, SPIE, Bellingham, Washington, USA, 2005.

Brion, J., Chakir, A., Charbonnier, J., Daumont, D., Parisse, C., and Malicet, J.: Absorption spectra measurements for the ozone molecule in the 350-830 nm region, J. Atmos. Chem., 30, 291-299, 10.1023/a:1006036924364, 1998.

Clifford, S. F.: Temporal-frequency spectra for a spherical wave propagating throught atmospheric turbulence, J. Opt. Soc. Am, 61, 1285-1292, 1971.

Consortini.A, Ronchi, L., and Stefanut.L: Investigation of atmospheric turbulence by narrow laser beams, Appl. Opt., 9, 2543-2547, 10.1364/ao.9.002543, 1970.

De Bruin, H. A. R., and Evans, J. G.: Long path scintillometry: a brief review, in: Remote Sensing and Hydrology, edited by: Neale, C. M. U., and Cosh, M. H., IAHS Publication, Wallingford, UK, 180-183, 2012.

Ding, Y. H., and Liu, Y. J.: Analysis of long-term variations of fog and haze in China in recent 50 years and their relations with atmospheric humidity, Science China: Earth Sciences, 57, 36-46, 2014.

Evans, J. G., and De Bruin, H. A. R.: The Effective Height of a Two-Wavelength Scintillometer System, Bound-Lay. Meteorol., 141, 165-177, 10.1007/s10546-011-9634-0, 2011.

Fiddler, M. N., Begashaw, I., Mickens, M. A., Collingwood, M. S., Assefa, Z., and Bililign, S.: Laser Spectroscopy for Atmospheric and Environmental Sensing, Sensors, 9, 10447-10512, 10.3390/s91210447, 2009.

Filho, F. C. M., Jayasuriya, D. A. R., Cole, R. S., and Helmis, C. G.: Spectral density of millimeter wave amplitude scintillations in an absorption region, IEEE T. Antenn. Propag., 31, 672-676, 1983.

Ishimaru, A.: Wave propagation and scattering in random media, Oxford University Press New York, 1997.

Jarvi, L., Rannik, U., Mammarella, I., Sogachev, A., Aalto, P. P., Keronen, P., Siivola, E., Kulmala, M., and Vesala, T.: Annual particle flux observations over a heterogeneous urban area, Atmos. Chem. Phys., 9, 7847-7856, 2009.

Lou, S., Liao, H., and Zhu, B.: Impacts of aerosols on surface-layer ozone concentrations in China through heterogeneous reactions and changes in photolysis rates, Atmos. Environ., 85, 123-138, 10.1016/j.atmosenv.2013.12.004, 2014.

Martensson, E. M., Nilsson, E. D., Buzorius, G., and Johansson, C.: Eddy covariance measurements and parameterisation of traffic related particle emissions in an urban environment, Atmos. Chem. Phys., 6, 769-785, 2006.

Nebuloni, R.: Empirical relationships between extinction coefficient and visibility in fog, Appl. Opt., 44, 3795-3804, 10.1364/ao.44.003795, 2005.

Nieveen, J. P., Green, A. E., and Kohsiek, W.: Using a large-aperture scintillometer to measure absorption and refractive index fluctuations, Bound-Lay. Meteorol., 87, 101-116, 1998.

Ott, R. H., and Thompson Jr., M. C.: Atmospheric Amplitude Spectra in an Absorption Region, IEEE T. Antenn. Propag., 16, 329-332, 1978.

Rao, R.: Modern Atmospheric Optics, Science Press, Beijing, 2012.

Raut, J. C., and Chazette, P.: Vertical profiles of urban aerosol complex refractive index in the frame of ESQUIF airborne measurements, Atmos. Chem. Phys., 8, 901-919, 2008.

Ripamonti, G., Jarvi, L., Molgaard, B., Hussein, T., Nordbo, A., and Hameri, K.: The effect of local sources on aerosol particle number size distribution, concentrations and fluxes in Helsinki, Finland, TELLUS B, 65, 19786, 10.3402/tellusb.v65i0.19786, 2013.

Solignac, P. A., Brut, A., Selves, J. L., Beteille, J. P., and Gastellu-Etchegorry, J. P.: Attenuating the Absorption Contribution on C-n2 Estimates with a Large-Aperture Scintillometer, Bound-Lay. Meteorol., 143, 261-283, 10.1007/s10546-011-9692-3, 2012.

Stull, R. B.: An Introduction to Boundary Layer Meteorology, Kluwer Academic Publishers, Boston, USA, 1988.

Tatarskii, V. I.: Wave Propagation in a Turbulent Medium, McGraw-Hill Book Company Inc., New York, 1961.

van Dinther, D., Hartogensis, O. K., and Moene, A. F.: Crosswinds from a Single-Aperture Scintillometer Using Spectral Techniques, J. Atmos. Ocean. Tech., 30, 3-21, 10.1175/jtech-d-12-00069.1, 2013.

Vogt, M., Nilsson, E. D., Ahlm, L., Martensson, E. M., and Johansson, C.: The relationship between 0.25-2.5 mu m aerosol and CO2 emissions over a city, Atmos. Chem. Phys., 11, 4851-4859, 10.5194/acp-11-4851-2011, 2011.

Formatted: Font: 9 pt, No underline, Font color: Black, Do not check spelling or grammar

Wang, T. I., Ochs, G. R., and Clifford, S. F.: Saturation-resistant optical scintillometer to measure Cn2, J. Opt. Soc. Am, 68, 334-338, 1978.

Wyngaard, J. C., Izumi, Y., and Collins, S. A.: Behavior of refractive-index-structure parameter near ground, J. Opt. Soc. Am, 61, 1646-1650, 10.1364/josa.61.001646, 1971.

Yuan, R., Sun, J., Luo, T., Wu, X., Wang, C., and Fu, Y.: Simulation study on light propagation in an anisotropic turbulence field of entrainment zone, Opt. Express, 22, 13427-13437, 2014.

Zhang, X., Huang, Y., Rao, R., and Wang, Z.: Retrieval of effective complex refractive index from intensive measurements of characteristics of ambient aerosols in the boundary layer, Opt. Express, 21, 17849-17862, 10.1364/oe.21.017849, 2013.

Formatted: Indent: Left: 0", Hanging: 1.35 ch

Formatted: No underline, Font color: Black

Formatted: Centered

Formatted: No underline, Font color: Black

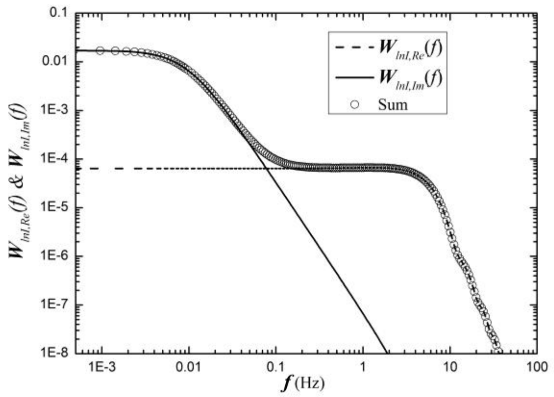

Figure 1. The theoretical temporal spectral densities~~y~~ ($W_{lnI,Re}(f)$ and $W_{lnI,Im}(f)$) of the logarithmic light intensity fluctuations ~~caused by~~due to the real and imagery parts of the ~~refractive index~~ARISP (see text for the parameter values used in the calculation).

Formatted: No underline, Font color: Black

Formatted: No underline, Font color: Black

Formatted: No underline, Font color: Black

Formatted: No underline, Font color: Black

Formatted: No underline, Font color: Black

Formatted: No underline, Font color: Black

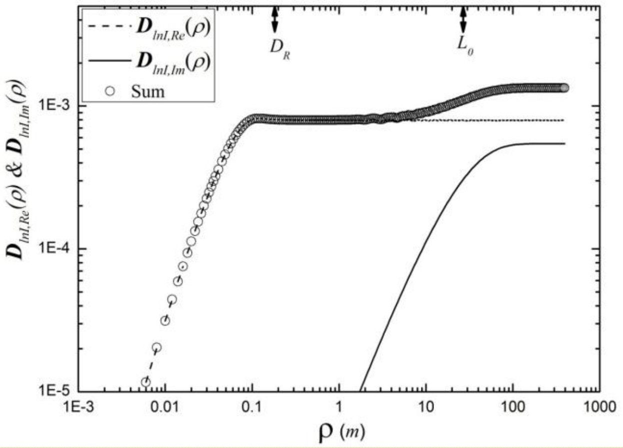

Figure 2. The ~~calculated~~ temporal structure functions, ($D_{lnI,Re}(\rho)$ and $D_{lnI,Im}(\rho)$) of the logarithmic light intensity fluctuations ~~caused by~~due to the real and imagery parts of the ~~refractive index~~ARISP, calculated with the same parameters ~~as~~ used in Fig. 1. The ~~Two~~ two arrows in the figure denote the values of diameter of transmitter (or receiver) and the outer scale ~~so as~~ to ~~help~~ asist with comparisons ~~of~~ to different scales.

Formatted: No underline, Font color: Black

Formatted: No underline, Font color: Black

Formatted: No underline, Font color: Black

Formatted: No underline, Font color: Black

Formatted: No underline, Font color: Black

Formatted: No underline, Font color: Black

Formatted: No underline, Font color: Black

Formatted: No underline, Font color: Black

Formatted: No underline, Font color: Black

Formatted: No underline, Font color: Black

Formatted: No underline, Font color: Black

Formatted: No underline, Font color: Black

Formatted: No underline, Font color: Black

Formatted: No underline, Font color: Black

Figure 3. Photographs of the measurement site, (a) ~~map~~ Map of Hefei ~~city~~City ~~,~~ and (b) Expanded view of the measurement sites ~~in~~ on the USTC campus, which is marked with the rectangle in (a). Point P in (a) indicates ~~for~~ the site from which~~for~~ visibility measurements were obtained.~~;~~ Points A and B in (b) show~~s~~ the locations of the transmitter and receiver, respectively. Point C in (b) ~~indicates~~ marks the meteorological tower position. There are 4 heavy traffic roads surrounding the measurement site.

Formatted: No underline, Font color: Black

Formatted: No underline, Font color: Black

Formatted: No underline, Font color: Black

Formatted: No underline, Font color: Black

Formatted: No underline, Font color: Black

Formatted: No underline, Font color: Black

Formatted: No underline, Font color: Black

Formatted: No underline, Font color: Black

Formatted: No underline, Font color: Black

Formatted: No underline, Font color: Black

Formatted: No underline, Font color: Black

Formatted: Centered

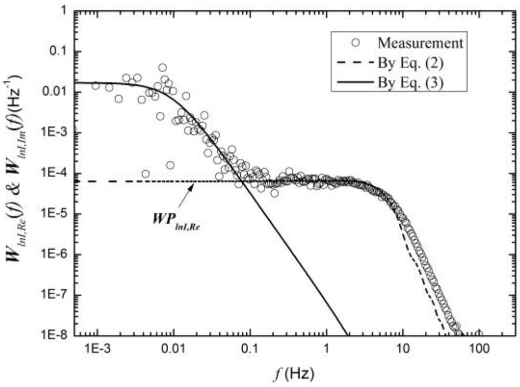

Formatted: No underline, Font color: Black

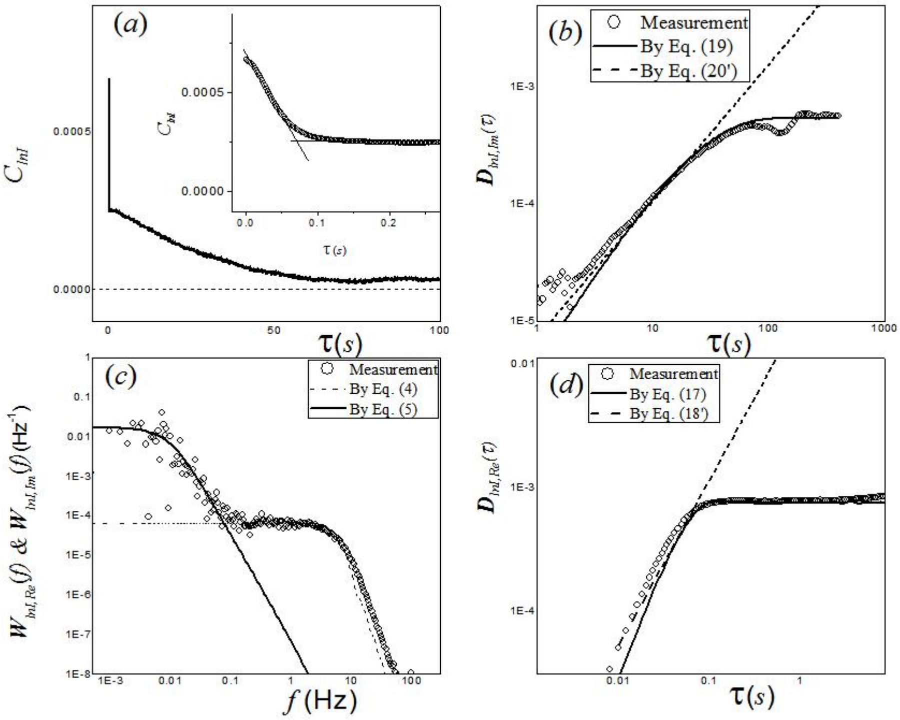

Figure 4: ~~Parameters derived from a~~ LAS observation ~~example~~ at 08:30 LT on 15 January 2014 used to derive spectral parameters. A theoretical calculation is shown for comparison.~~,~~ ~~08:30 and comparison with theory. (a) Time delay auto-correlation of the logarithmic light intensity fluctuations.(b) Structure function of the logarithmic light intensity fluctuations caused by the imagery part of the refractive index (circles) and the theoretical curves (solid~~

Formatted: No underline, Font color: Black

Formatted: No underline, Font color: Black

Formatted: No underline, Font color: Black

~~line and dash line).~~ ~~(c)~~ The temporal spectral density ($W_{lnI,Re}(f)$ and $W_{lnI,Im}(f)$) of the logarithmic light intensity fluctuations (circles) and the theoretical curves associated with the real and imagery parts of the ~~refractive index~~ARISP (solid line and dashed line).~~,~~ respectively) are plotted. $WP_{lnI,Re}$ refers to the spectral density of the plateau region described by Eq. (6) in the text.~~ (d) Structure function of the logarithmic light intensity fluctuations contributed by the real part of the refractive index (circles) and corresponding theoretical curves (solid line and dash line).~~

Formatted: No underline, Font color: Black

Formatted: No underline, Font color: Black

Formatted: No underline, Font color: Black

Formatted: No underline, Font color: Black

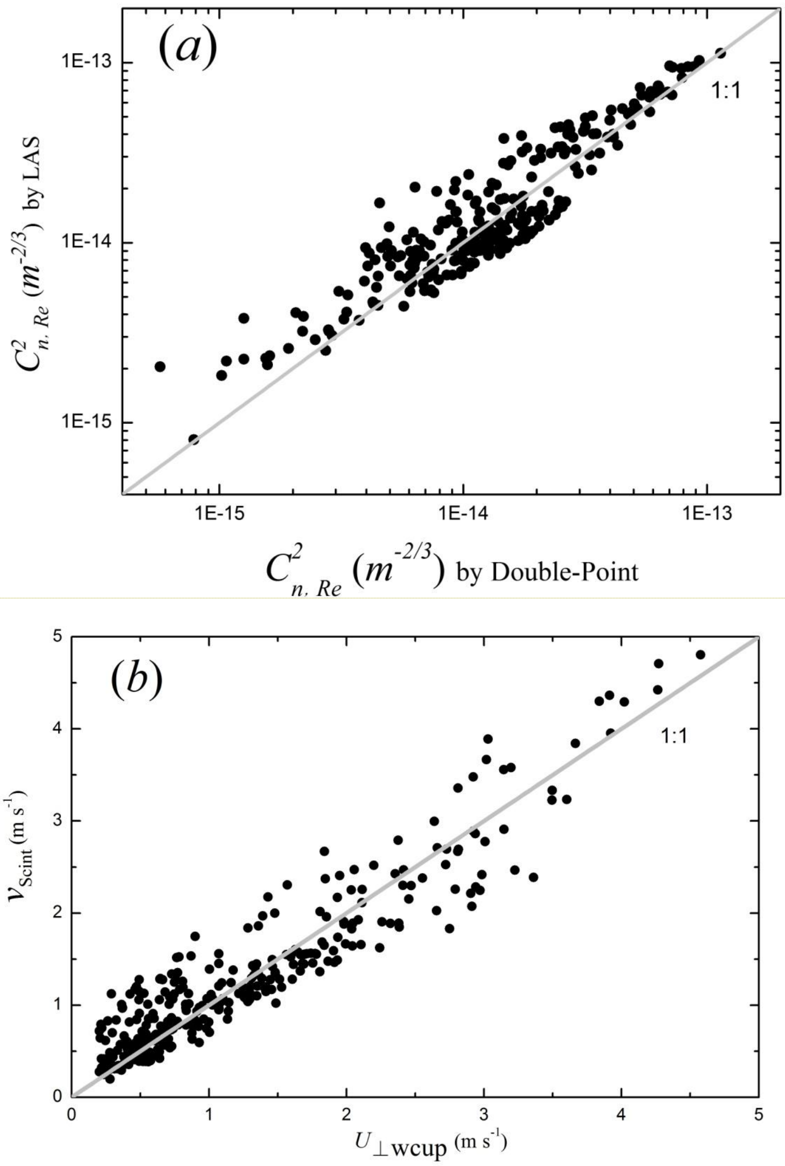

Formatted: No underline, Font color: Black

Formatted: No underline, Font color: Black

~~Figure 5.Comparisons of the real part of the ARISP and transverse wind speed between two methods. (a) Comparison of the real part of the ARISP between the Double-Point measurements and LAS measurements. (b)Comparison of transverse wind speeds between cup anemometer and LAS measurements.~~

Formatted: No underline, Font color: Black

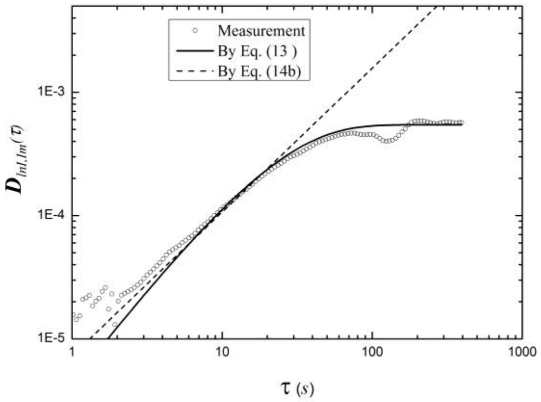

Figure 5.LAS observation (obtained at the same time as that shown in Fig. 4) used to derive the imaginary part of the ARISP and comparison with the theoretical results. The structure function of the logarithmic light intensity fluctuations caused by the imaginary part of the refractive index (circles) and the theoretical curves (solid line and dash line) are plotted.

Formatted: No underline, Font color: Text 1

Formatted: No underline, Font color: Black

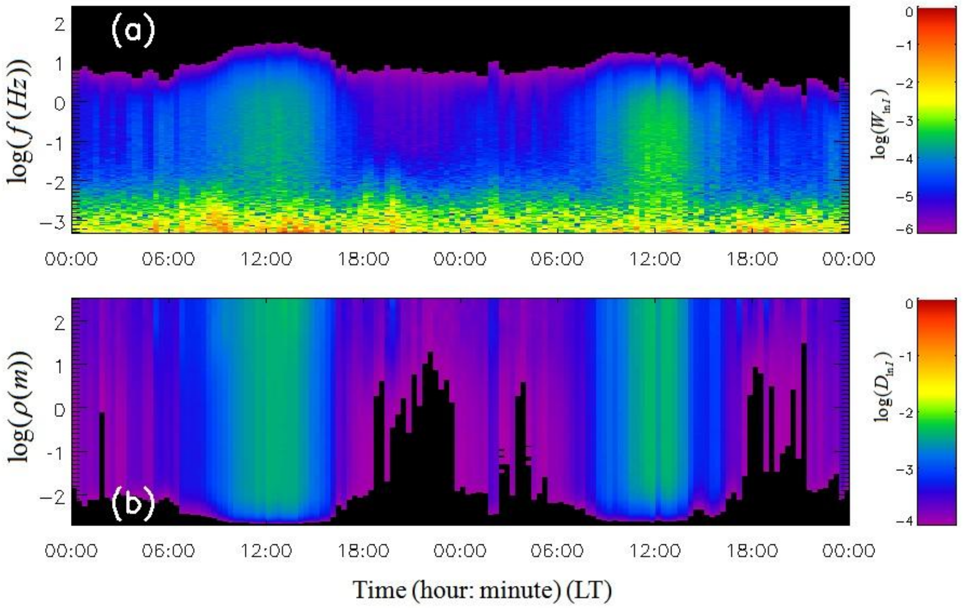

Figure 6. The evolution of the *(a)* temporal spectral density~~ *(a)*~~ and *(b)* structure function of the logarithmic light intensity fluctuations ~~(b)~~observed during 15-16 January 2014. In (a), the two-dimensional colour of the contour denotes the logarithm of the temporal spectral density of the logarithmic light intensity fluctuations according to the colour bar shown ~~at~~on the right. In (b), the two-dimensional colour contour denotes the logarithm of structure function of the logarithmic light intensity fluctuations according to the colour bar shown ~~at~~ on the right. The black grids indicate~~ the~~ values that below ~~less than~~ the minimum of the colour scale.

Formatted: No underline, Font color: Black

Formatted: No underline, Font color: Black

Formatted: No underline, Font color: Black

Formatted: No underline, Font color: Black

Formatted: No underline, Font color: Black

Formatted: No underline, Font color: Black

Formatted: No underline, Font color: Black

Formatted: No underline, Font color: Black

Formatted: No underline, Font color: Black

Formatted: No underline, Font color: Black

Formatted: No underline, Font color: Black

Formatted: No underline, Font color: Black

Formatted: No underline, Font color: Black

Formatted: No underline, Font color: Black

Formatted: No underline, Font color: Black

Formatted: No underline, Font color: Black

Formatted: No underline, Font color: Black

Formatted: No underline, Font color: Black

Formatted: No underline, Font color: Black

Formatted: No underline, Font color: Black

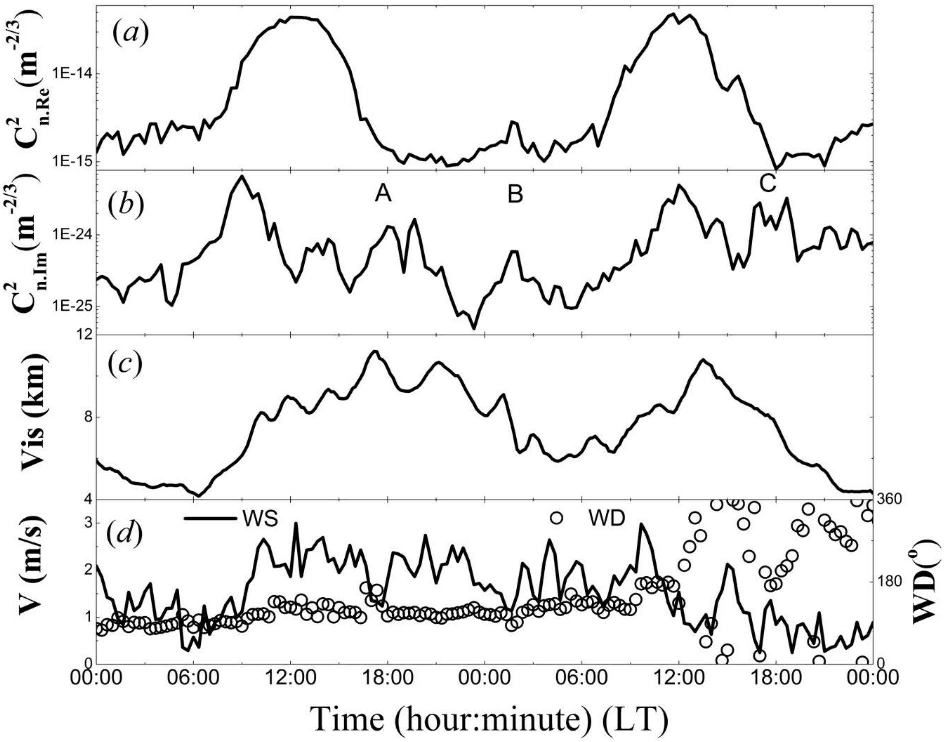

Figure 7.T~~he t~~emporal variations of the (a) real part of the ARISP~~,~~ (~~a~~b)~~,~~ ~~the~~ imaginary part of the ARISP(b), (c) visibility~~ (c),~~ and (d) wind speed and direction~~ (d)~~observed during 15-16 January 2014. The points labelled A, B and C in panel (b) highlight the three periods with large values for the imaginary part of the ARISP other than the two daily maximum. Details can be found in the text.

Formatted: No underline, Font color: Black

Formatted: No underline, Font color: Black

Formatted: No underline, Font color: Black

Formatted: No underline, Font color: Black

Formatted: No underline, Font color: Black

Formatted: No underline, Font color: Black

Formatted: No underline, Font color: Black

Formatted: No underline, Font color: Black

Formatted: No underline, Font color: Black

Formatted: No underline, Font color: Black

Formatted: No underline, Font color: Black